Oxidative potential apportionment of atmospheric PM$_1$: A new approach combining high-sensitive online analysers for chemical composition and offline OP measurement technique

Julie Camman[1,2,†], Benjamin Chazeau[1,3,†], Nicolas Marchand[1], Amandine Durand[1], Grégory Gille[4],
Ludovic Lanzi[4], Jean-Luc Jaffrezo[2], Henri Wortham[1] and Gaëlle Uzu[2]

[1]Aix Marseille Univ, CNRS, LCE, UMR 7376, 13331 Marseille, France
[2]Univ. Grenoble Alpes, CNRS, IRD, IGE (UMR 5001), 38000 Grenoble, France
[3]Laboratory of Atmospheric Chemistry, Paul Scherrer Institute, 5232 Villigen, Switzerland
[4]AtmoSud, Regional Network for Air Quality Monitoring of Provence-Alpes-Côte-d'Azur, Marseille, France
† These authors contributed equally to this work

Correspondence to: Benjamin Chazeau (benjamin.chazeau@univ-amu.fr)

Abstract. Source apportionment models were widely used and/or atmospheric chemical processes. These technics are necessary to target the sources affecting air quality and to design effective mitigation strategies. More, the evaluation of the toxicity of airborne particulate matter gains interest as the PM concentrations classically measured appear insufficient to characterise the human health impact. Oxidative Potential (OP) measurement have recently been developed to quantify the PM capability to induce an oxidative imbalance in lungs. As a result, this measurement unit could be a better proxy than PM mass concentration to represent PM toxicity. In the present study, two source apportionment analyses were performed using Positive Matrix Factorization (PMF) from organic aerosol (OA) mass spectra measured at 15 min time resolution using a Time of Flight-Aerosol Chemical Speciation Monitor (ToF-ACSM) and from 19 trace elements measured on an hour basis using an online metals analyser (Xact). The field measurements were carried out in summer 2018. While it is common to perform PMF studies individually on ACSM and more recently on Xact datasets, here we used a two-step methodology leading to a complete PM$_1$ source apportionment. The outputs from both OA PMF and Xact PMF, the inorganic species concentrations from the ACSM and the black carbon (BC) fractions (fossil fuel and wood burning) measured using an Aethalometer (AE33) were gathered into a single dataset and subjected to a combined PMF analysis. In overall, 8 factors were identified, each of them corresponding to a more precise source than performing the previous single PMF analyses. The results show that besides the high contribution of secondary ammonium sulfate (28%) and organic nitrate (19%), about 50% of PM$_1$ were originated from combustion processes (traffic, shipping, industrial, cooking and biomass burning emissions). Simultaneously, PM$_1$ filters were collected during the experimental period on a 4 hours sampling basis. On these filters, two acellular OP assays were measured (dithiothreitiol; OP$_{DTT}$ and ascorbic acid; OP$_{AA}$) and an inversion method is applied on factors issued from all PMFs to assess contributions of the PM sources to the OP. This work highlights the sensitivity of OP$_{AA}$ toward industrial and dust resuspension sources and those of OP$_{DTT}$ toward secondary ammonium sulfate, shipping and biomass burning.

1. Introduction

Airborne particulate matter is a significant contributor to air pollution, leading to adverse effects on ecosystems, climate
35 stability and environment (Beelen et al., 2014; Cohen, 2017; Jacob, 1999). Air quality is currently a major public health
outcome and is responsible of 4.2 million premature deaths worldwide each year (WHO, 2021) . More worryingly, this figure
is expected to double by 2050 (Lelieveld et al., 2015). However, the links between air pollution and human health effects are
not fully understood yet, but particulate matter appears to be a key pollutant in aerosol toxicity (Medina S. et al., 2016; Zhang
et al., 2016). Depending on their size and chemical composition, PM may cause high damage on pulmonary cells due to their
40 ability to penetrate more or less deeply in the organism and to induce inflammatory responses on lung cells (Strak et al., 2012).
There has been a growing interest in recent years in submicron aerosol PM_1 which are deposited deeply in the respiratory
system, reaching the alveoli of the lungs (Sturm, 2020). PM_1 are associated to the physicochemical processing of compounds
also resulting from anthropogenic sources, mainly combustion sources, and are known to contribute to health impact of the
PM (Grigas et al., 2017; Manigrasso et al., 2020).

45 Although an increasing number of studies investigated the potential effects of submicronic particles on the risk of respiratory
diseases, this subject still represents a research line that needs further toxicological and epidemiological studies (Hu et al.,
2022). It was recently shown that they are strongly linked to the occurrence of cardiovascular disease, perhaps due to its higher
surface-to-volume ratio (Münzel et al., 2022). While the air quality guidelines regarding PM levels were recently updated for
PM_{10} and $PM_{2.5}$ (WHO, 2023), no regulation for PM_1 has yet been established, and several studies suggest their monitoring
50 should be considered with this respect (Kumar et al., 2010).

While all mechanisms leading to the toxicity of airborne particles are not fully established yet, it is generally believed that the
activity of Reactive Oxygen Species (ROS) could play an important role. These chemical species carried or induced in the
lung are suspected of disrupting the natural redox balance, causing oxidative stress, a key factor in the inflammatory response
in the organism, ultimately leading to diseases such as asthma or chronic bronchitis (Abrams et al., 2017; Dellinger et al.,
55 2001; Møller, 2014; Pope, 2004). Thus, new approaches have been investigated for a couple of decades to better quantify
oxidative stress and ultimately the impact on population of exposure to airborne particulate pollution. Indeed, the measurement
of oxidative potential (OP) of PM is seen as a new promising metric and probably a better representative proxy of health
impacts than the PM mass concentration, as it quantifies the ability to generate ROS *in vivo*. It integrates many properties of
PM important for the interactions with lung fluid, such as size distribution, specific surface area or PM chemical composition
60 (Ayres et al., 2008). Indeed, changes in chemical composition of aerosol and consequently the type of sources from which they
are emitted may lead to a large difference in airborne particles toxicity (Boogaard et al., 2012). Furthermore, previous studies
showed the interest in the fine mode in understanding oxidative effects of PM (Chen et al., 2017).

An active field of research for Air Quality is understanding the emission sources of PM through source apportionment
techniques, using approaches such as statistical receptor models (e.g. chemical mass balance (CMB) or positive matrix
65 factorization (PMF)) (Paatero and Tapper, 1994). Widely used in the community, PMF can be based either on data from online

analysers such as Aerosol Mass Spectrometer (AMS) and Aerosol Chemical Speciation Monitor (ACSM) which allow the resolution of organic mass spectra with high sensitivity (Bozzetti et al., 2017; Chen et al., 2022; Crippa et al., 2013b) or from off-line filters analyses (Borlaza et al., 2021b, a).

Several ways have been explored to combined datasets from several online analysers to perform PMF. Some studies proposed
70 to combine high resolution AMS and proton-transfer-reaction mass spectrometer (PTR-MS) measurements to refine the links between particle phase organics and their precursors (Crippa et al., 2013a; Slowik et al., 2010). Some others performed source apportionment by including both organic and inorganic fractions from the AMS (Äijälä et al., 2019; McGuire et al., 2014; Sun et al., 2012), improving the factors resolution and their chemical nature. More recently, Zografou et al. (2022) performed PMF analysis on combined organic and inorganic year-long dataset from a ToF-ACSM. Tong et al. (2022) combined into a single
75 dataset AMS and extractive electrospray ionisation time-of-flight mass spectrometer (EESI-ToF) measurements providing an optimised identification and quantification of the organic factors, more specifically the SOA fraction. Nursanto et al. (2023) also tried an hybrid approach by combining this time organic aerosol concentrations from a ToF-ACSM with the particle size distribution from a Scanning Mobility Particle Sizer (SMPS) and resolved organic factors related to new particle formation and growth.

80 However, a lot of efforts remain for combining instruments datasets and apportion the sources of the total PM_1 fraction. A multi-time resolution approach was suggested by Via et al. (2023) mixing PM_1 data from online analysers and offline filters. Belis et al. (2019) conducted three separated PMF analyses (on offline filters data, online organic data and online inorganic species) which produce reference profiles to constrain a fourth PMF with combined online data. Petit et al. (2014) also followed a multi-step methodology (PMF²) consisting in the use of results from the first PMF runs as inputs for their combined PMF
85 using ACSM and AE33 data. To our knowledge, there is no other study performing such PMF^2 approach, in particular for all PM_1 components. The current study addresses this challenge by intending a PMF^2 method for the PM_1 fraction measured with online analysers (i.e. ToF-ACSM, Xact 625i and aethalometer) at high time resolution (<1h).

While the study of the relationship between the OP and single compounds is a step forward in understanding the chemical mechanisms involved, it seems unrealistic to characterise the OP of the aerosol as a whole in this way, given the myriad of
90 chemical elements that make up the aerosol. A more integrative approach is to consider OP sources since aerosol is a complex mixture where synergistic and antagonistic effects can occur (Yu et al., 2018). This allows an estimation of intrinsic OP of sources but also of their contribution to population's health exposure, which is more practical for adapting air quality management policies (Borlaza et al., 2018; Calas et al., 2019; Fang et al., 2016; Grange et al., 2022; Verma et al., 2014; Weber et al., 2018; Yu et al., 2019).

95 Major insights have been gained from OP measurements on filters. Many studies, based on filters collected on different sites, have established associations between OP and PM sources, thus improving the understanding health impact of specific types of airborne particles (Borlaza et al., 2021a; Daellenbach et al., 2020; Fang et al., 2016; Weber et al., 2021). However, the next step is to develop online OP measurement to understand one-time extreme events and ultimately allow near real time (NRT) OP acquisition for a better air quality management.

To make progress in this direction, we propose here to investigate the submicron aerosol -highly considered in health impact (Lin et al., 2020)- sources contributing most to two type of OP (ascorbic acid assay (OP_{AA}) and Dithiotreitol assay (OP_{DTT})) in a challenging environment, the Marseille area. Effectively, the activity of the industrial-port complex and several industrial areas close to this high-urbanized city combined with specific meteorological conditions -wind regimes and significant photochemistry in summer- implies frequent pollution episodes (Chazeau et al., 2022, 2021; Salameh et al., 2018). A challenging double PMF method using chemical online analysers (ToF-ACSM, Xact and aethalometer) is proposed as a first step. High-frequency acquisition of OP observations with filter sampling every 4h for 7 weeks were then coupled to this data. On this basis, an OP source apportionment using a multilinear regression approach is provided. This method allows an estimation of the oxidizing capacity of each µg of PM_1 from the identified emission sources but also the relative contribution of each source to OP_{AA} and OP_{DTT} on a 4h basis. The complementarity of these assays gives a broader and more representative view of the PM_1 health impact.

2. Material and methods

2.1 Site and sampling

Site sampling

The Marseille-Longchamp supersite is an urban background site of Marseille -2nd most populated city in France (about 870 000 inhabitants, with a density of 3600 inhabitant/km² in 2019). The site is located in the heart of the Longchamp park, in the 4th district of Marseille (43°18'20" N; 5°23'41; m a.s.l.). Figure 1 shows the site location in the city and main areas in the surroundings with the maritime port of Marseille within 2km and industrial areas within 30 km with petroleum refining, coke production plants, and steel facilities activities (Salameh et al., 2018). In addition to shipping and industrial local sources, Marseille suffers from the second largest traffic congestion in France, generating a year-round source of background traffic (Chazeau et al., 2021). The location of the city also leads to influences of natural and biogenic emissions as marine aerosol, terrestrial vegetation, saharian dust or crustal dust. Finally, secondary organic aerosol (SOA) formation events and high ozone concentrations formed by intense photochemistry are frequent during warm periods in the area (El Haddad et al., 2013; Flaounas et al., 2009).

Sampling campaign

The sampling campaign and site have been detailed elsewhere (Chazeau et al., 2022). Briefly, the field work took place during the summer of 2018 over a seven-week period (from 11th July to 1st September 2018). The sampling station was equipped with a range of analytical instruments for characterisation of submicron aerosol: a Time-of-flight Aerosol Chemical Speciation Monitor (ToF-ACSM; Fröhlich et al., 2013) to measure in near real-time (10-min resolution) the chemical composition of non-refractory PM_1 (Organic aerosol, NH_4^+, NO_3^-, SO_4^{2-} and Cl^-), a dual spot Magee Scientific AE33 aethalometer (Drinovec et al., 2015) equipped with a $PM_{2.5}$ cut-off inlet to measure the equivalent black carbon concentrations (BC: with a distinction

between BC_{FF} and BC_{WB} origins) at a 1-min resolution, and a Xact625i (Cooper Environmental) to measure a user-defined list of 25 PM_1 trace elements with a time resolution of 60 min. PM_1, $PM_{2.5}$ and PM_{10} mass concentrations were determined with an optical particle counter (FIDAS 200; PALAS). A 3D sonic anemometer for temperature, wind direction and velocity

135 measurements and O_3, NO_x and SO_2 analysers are also amongst the permanent instruments of the station. Finally, PM_1 collection for OP analysis was performed on 150 mm diameter quartz fibre filters (Whatman Tissuquartz) pre-heated at 500°C during 8 hours), using a high-volume aerosol sampler (HiVol, Digitel DA80) at a flow rate of 30 $m^3.h^{-1}$. A total of 90 samples and 4 blank filters were collected between 11th July and 25th July 2018, with a time resolution of 4 h. All procedurals care for filter handling, sampling and storage were taken to avoid contamination and evolution of the filter deposit after sampling

140 (Weber et al., 2018).

All the instruments ran acquisitions during the whole campaign period (i.e. July 11th July to September 1st 2018). However, it should be noted that ToF-ACSM stopped between 12th July 2018 19:00 – 13th July 2018 03:00 (UTC) and between 14th July 2018 15:00 – 15th July 2018 03:00 (UTC), which implies a number of filter samples reduced to 83 instead of 90 for OP deconvolution model discussed below.
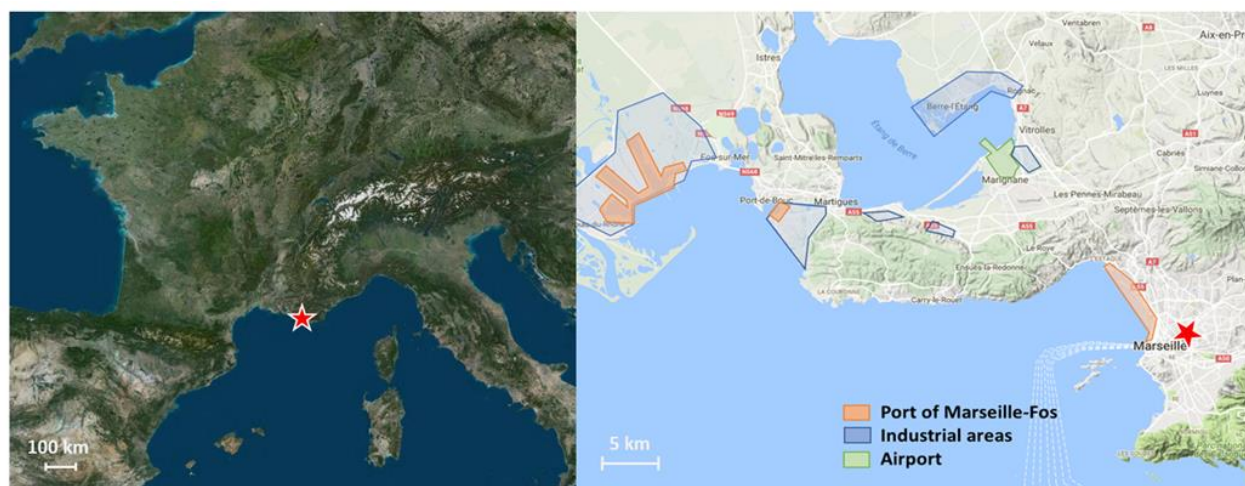
145

Figure 1. Location of Marseille-Longchamp supersite and localization of main industrial areas around Marseille, France (© PlaneteObserver, Geoportail / © Google Maps).

2.2 OP analysis

OP was assessed by the depletion rate of anti-oxidant compounds, using the two methods with Dithiothreitol (DTT) and

150 ascorbic acid (AA) (Calas et al., 2019, 2018, 2017). DTT depletion in contact with PM extracts was determined by dosing the remaining amount of DTT with dithionitrobenzoic acid (DTNB) at different reaction times (0, 15 and 30 min), and absorbency was measured at 412 nm using a plate spectrophotometer (Tecan, M200 Infinite). Briefly, 25 µM of DTT and phosphate buffer react for 30 min with PM suspension at 25 µg.mL^{-1} in a simulated lining fluid. The AA assay is a simplified version of the synthetic respiratory tract lining fluid (RTLF) assay (Kelly, 2003), where only AA is used. A mix of 80 µL of PM suspension

155   with 24 nmol of AA (100 µL of 0.24 mM AA solution in Milli-Q water) is used, and AA depletion was read continuously for
30 min by absorbency at 265 nm (TECAN, M1000 Infinite). The depletion rate of AA was determined by linear regression of
the linear section data. For both assays, the 96-well plate was auto-shaken for 3 s before each measurement and kept at
physiological conditions (37.4°C).

Three filter blanks (laboratory blanks) and three positive controls (1,4-naphthoquinone, 24.7 µmol.L^{-1}) were included in each

160   plate (AA and DTT). The average values of these blanks were then subtracted from the sample measurements of the given
plate. The detection limit value was defined as three times the standard deviation of laboratory blank measurements (laboratory
blank filters in Gamble + DPPC solution). Three replicates are performed with two absorbance measurements at each time.
The short duration of the sampling time (4 h), the type of PM fraction (PM$_1$) and consequently the low mass recovered on each
filter resulted in some OP replicates measurements below the detection limit, implying highest uncertainties as usual for such

165   measurements (Calas et al., 2018; Weber et al., 2021) in these results. A propagation of these uncertainties was carried out (in
average 15% of the OP measurement) to deal with it. Hereafter, the OP normalized in volume relative to AA assay and DTT
assay are denoted OP$_{vAA}$ and OP$_{vDTT}$.

2.3 Source apportionment using Positive Matrix Factorization (PMF)

Source apportionment was performed through Positive Matrix Factorization (PMF; Paatero and Tapper, 1994) method using

170   the multi-linear engine (ME-2) solver (Paatero, 1999) and run within the Source Finder Professional (SoFi Pro) software
(Datalystica Ltd., Villigen, Switzerland; Canonaco et al., 2021, 2013). PMF is a bilinear unmixing model widely used to
determine the atmospheric aerosol sources based on online measurements (Canonaco et al., 2021; Chazeau et al., 2022; Chen
et al., 2022). The equation is described as follow:

$$x_{i,j} = \sum_{k=1}^{n} g_{i,k} \cdot f_{k,j} + e_{i,j} \tag{1}$$

175   With $x_{i,j}$ a non-negative matrix of measurements which is factorized into $g_{i,k}$ the factor time series, $f_{k,j}$ the factor profiles and
$e_{i,j}$ the model residuals. The index i, j, k and n are the time, variables, discrete factor numbers and total number of factors in a
solution, respectively.

ME-2 solves the model solution by using a least squares algorithm to iteratively minimize the following object function Q
defined as the sum of the squared model residuals weighted by their respective uncertainties (σ_{ij}):

180    $$Q = \sum_i \sum_j \left(\frac{e_{ij}}{\sigma_{ij}}\right)^2 \tag{2}$$

Generally, the PMF model doesn't result in a mathematically unique solution as a multiple combination of $f_{k,j}$ and $g_{i,k}$ may
provide a similar value of Q. ME-2 allows then to introduce a-priori information in the model using known source profiles or
time series to orient solutions towards environmentally meaningful rotations (Paatero, 1999; Paatero and Hopke, 2009). An
advantage of SoFi Pro is that it enables to control the rotational ambiguity of the solution by applying constraints with the a-

185   value approach (Canonaco et al., 2013):

$$f_{kj} = f'_{kj} \pm a \cdot f'_{kj} \qquad (3)$$

$$g_{ik} = g'_{ik} \pm a \cdot g'_{ik} \qquad (4)$$

Where the scalar a defined the range (between 0 and 1) to which f'_{kj} and g'_{ik} can vary from the known input profile (f_{kj}) or time series (g_{ik}).

190 In the current study, source apportionment was conducted using PMF model on three distinct datasets. In the first two analyses, PMF was applied separately to the OA dataset (PMF$_{organics}$) and Xact dataset (PMF$_{metals}$). As a second step, the outputs from the previous source apportionment analyses, the inorganic species concentrations from the ToF-ACSM measurements (NO$_3^-$, NH$_4^+$, SO$_4^{2-}$ and Cl$^-$) and the deconvolved BC sources (BC$_{FF}$ and BC$_{WB}$) concentrations from the AE33 were combined into a single dataset to perform a total PM$_1$ source apportionment (PMF$_{PM1}$).

2.4 PMFs preparation and optimization

2.4.1 OA dataset

ACSM data were acquired with the Igor-based Acquility v2.1.4 software and analysed with Tofware v3.2 also developed in Igor Pro (Wave Metric inc., Lake Oswego, Oregon, USA). The data treatment including ionisation efficiency (IE) and relative ionisation efficiency (RIE) calibrations, collection efficiency (CE) correction and detection limits determination is detailed in 200 Chazeau et al. (2021). The complete PMF methodology and optimization applied to OA mass spectra at MRS-LCP are described in a dedicated paper (Chazeau et al., 2022) and we will only provide a brief summary here. The model is performed on data input including 185 variables from m/z12 to m/z 214 and 4422 time steps (15 min intervals) from 1st July to 1st September 2018. The error matrix was exported from the Tofware software and the calculation included ion counting statistics, background errors, electronic noise and a minimum error from the measurement of a single ion.

205 A five-factors solution was resolved with three constrained and two unconstrained factors. Both hydrocarbon-like organic aerosol (HOA) and cooking-like organic aerosol (COA) factor profiles were constrained using the reference profiles from Ng et al. (2011) and Crippa et al. (2013b), respectively. Shipping/Industrial organic aerosol (Sh-IndOA) factor time series were constrained with the SO$_2$ concentrations as it is a specific proxy for these emissions in the Marseille area (El Haddad et al., 2013). The a-value ranges for these constraints were optimized based on some previous sensitivity analyses (Chazeau et al., 210 2022) and random a-values between 0-0.6, 0-0.2 and 0-0.2 for HOA, COA and Sh-IndOA, respectively, were retained. The two remaining factors corresponded to the secondary/oxygenated organic fraction separated in two components: a less oxidized organic aerosol (LOOA) and a more oxidized organic aerosol (MOOA) factors.

In order to explore the rotational ambiguity and statistical uncertainties of the PMF solution, a bootstrap resampling strategy is applied (Efron, 1979), where 100 repeated runs are performed to test the stability of the solution. The inspection of the 215 hundred generated runs was achieved based on a predefined criteria selection customized within SoFi Pro (Canonaco et al., 2021; Chazeau et al., 2022; Chen et al., 2022, 2021). First, three criteria are defined as acceptance thresholds to evaluate the quality of the PMF runs. The r Pearson correlation (denoted r hereafter) with BC$_{FF}$ for HOA, the ratio between lunch hours

(11h00 and 12h00 UTC) and the average background hours in the morning (06h00-08h00 UTC) for COA, and the r Pearson correlation with SO$_2$ for Sh-IndOA were used. Then, the monitoring of f43 intensity for LOOA and f44 intensity for MOOA

220 are used as repositioning criteria to avoid mixing of the unconstrained factors since they are not sorted automatically among the different PMF iterations. The bootstrapped runs fulfilling the criteria list were then averaged into a unique PMF solution.

2.4.2 Xact dataset

The PMF$_{metals}$ was performed on the Xact data matrix of hourly element concentrations from July 11th to September 1st 2018. First, some individual species were excluded to improve the quality of the analysis. Elements whose concentrations were below

225 their respective Minimum Detection Limit (MDL) more than 90% of the time were not included in the inputs (Fig. S1). The MDLs were provided by the manufacturer and are given in Table S1. From this approach, the following 17 elements remained: As, Br, Ca, Cd, Cr, Cu, Fe, K, Mn, Ni, Pb, Sb, Se, Sn, Ti, V and Zn. Co was also included in the inputs as it showed a good correlation with Ni element (R² = 0.5).

A PMF error matrix ($\sigma_{i,j}$) was estimated using the (Eq. 5) for concentrations greater than the MDL (Reff et al., 2007; Ryder

230 et al., 2020):

$$\sigma_{i,j} = \sqrt{MDL_i^2 + u_{i,j}^2} \qquad (5)$$

Where $u_{i,j}$ is a specific analytical uncertainty for each data point provided by the Xact. It includes both uncertainties of the sampling air volume and uncertainties of the mass spectra deconvolution calculated by the Xact software. For the concentrations below the MDL, the values were replaced by the MDL of metal divided by 2. The corresponding error is often

235 used to be set to 5/6 × MDL (Polissar et al., 1998). Since the relative error for each datapoint was most of the time less than 50%, Polissar et al. (1998) recommended to apply a relative error between 100% and 250% for values below the MDLs. In our dataset, some relative errors for data greater than the MDLs were much larger than 50%. Following Polissar et al. (2001), the elements were downweighted by using larger error estimates for values below the MDLs. The methodology and the PMF tests panel applied are described in the Supplement. All the data points with a signal-to-noise ratio (S2N) below 1 were

240 downweighted by adding a penalty function of 1/S2N to the error (Rai et al., 2020; Visser et al., 2015). The weighting is performed cell-wise as some variables had low average S2N but some high S2N periods.

Intense firework episodes were recorded during the French National Day celebration on 14th July. While it is common to exclude such episodes from the PMF analyses to reduce modelling uncertainties linked to very high concentrations (Ducret-Stich et al., 2013), some studies succeed in identifying a firework factor profile. Rai et al. (2020) performed a constrained PMF

245 analysis only on the firework hours and identified a firework factor based on the K/S elemental concentration ratio in black powder. The factor profile of fireworks was then constrained in the final complete dataset PMF analysis. Manousakas et al. (2022) ran a PMF on the entire dataset constraining all the source profiles except the fireworks factor and the time series of all sources. The fireworks time series were set to zero except during the corresponding events. In this study, we followed the same logic and the firework hours (13 July 20:00 UTC to 14 July 05:00 UTC; 14 July 20:00 UTC to 15 July 14:00 UTC) were

250   removed from the dataset to inspect the remaining sources. The PMF inputs without the firework points (WFP) consist in 1201 time points with 1h step and 18 elements. As a second step, PMF analyses were conducted only on Firework days (13 and 14 July) points (FDP) to determine a specific profile. The dataset represented 60 time points and 19 variables. In addition to the elements previously selected, Bi was included as it was exclusively associated to the firework events. Bi as bismuth trioxide form (Bi_2O_3) is commonly used instead of the toxic lead metals for crackling fireworks, the so-called "dragon's eggs" (Mohan,

255   2010; Perrino et al., 2011). Finally, the PMF was performed on the total dataset (1230 time points and 19 variables) by adding a constrained firework factor.

One important step is selecting the number of factors based on both mathematical diagnostics and environmental meaning of the factors. Solutions with a range of 1 to 8 factors were examined for the WFP dataset. The selection is achieved based on the changes in Q/Qexp ($\Delta Q/Q_{exp}$) and real and noisy unexplained variation (ΔUEV_{real}, ΔUEV_{noisy}) when increasing the number of

260   factor (Fig. S2). A large reduction of these values would indicate limited improvements of the model residuals and explained variability. There were no significant changes in ΔUEV_{real} and ΔUEV_{noisy} between 2 and 8 factors. However, $\Delta Q/Q_{exp}$ showed a decrease up to five factors meaning the changes in Q/Q_{exp} were very low. To relate the factors from the PMF with specific sources, the diurnal trends, time series of elements and comparison with some external tracers were examined. We could clearly identify five environmentally reasonable factors: dust resuspension, shipping, industrial, tire/brake wear and regional

265   background factors. Selecting the 6-factors solution results in an unresolved Br-rich factor which can't be attributed to a specific source or aerosol processes. Therefore, the 5-factors solution was chosen as the best representation of the data.

For the FDP dataset, the PMF analysis resolved the same five factors in addition to a firework factor. However, the analysis showed some mixing between the regional background and the firework factors due to the large contribution of K in both factors. To avoid this mixing, regional background profile was tightly constrained using the profile resolved with the WFP

270   dataset and an a-value of 0.1. The runs were repeated 50 times with a bootstrap resampling strategy to test the stability of the solution. This time a well-defined firework factor was resolved (Fig. S3) with an elemental composition in agreement with other studies (see section 3.2.2).

The averaged firework factor profile retrieved from the FDP dataset was used as a constraint for the complete dataset with a-values randomly initialised between 0 and 0.5 with an increment of 0.1. This initialisation is used to evaluate whether larger

275   deviations could improve the results (Canonaco et al., 2021). The factor time series were also constrained with similar a-values and set to 0 except during the firework events. The remaining factors were let unconstrained in the complete dataset solution. Similarly to the PMF$_{organics}$ methodology, 100 bootstrapped runs are conducted and a criteria-based selection is used to assess the quality and position of the PMF runs (Fig. S4). This statistical selection is described in the Supplement section.

2.4.3 Combined PM$_1$ dataset

280   Following the methodology described by Petit et al. (2014), we combined PMF outputs with the remaining chemical species of PM$_1$. Thus, the factors from both PMF$_{organics}$ and PMF$_{metals}$ were combined with BC_{FF}, BC_{WB}, NO_3^-, NH_4^+, SO_4^{2-} and Cl^- concentrations. The uncertainty matrix was constructed as following: uncertainties for the ToF-ACSM inorganic species were

exported with Tofware similarly to those for the organics; BC_{FF} and BC_{WB} uncertainties were estimated based on (Eq. 5) and (Eq. S1), with MDLs set to 0.1 for both species and $u_{i,j}$ the relative uncertainties set to 40% (Petit et al. 2014) multiplied by

285 the species concentrations; $PMF_{organics}$ and PMF_{metals} outputs errors were taken from the standard deviations of factors time series from the bootstrap analyses, which can be used as statistical uncertainties (Canonaco et al., 2021).

All the variables were synchronized to a 1h time resolution corresponding with the 4h time resolution of the filter sampling, and the missing measurement periods of each instrument were removed from the PMF analysis. The firework$_{metals}$ factor was excluded here as the ToF-ACSM was not running during the main active period of this event (i.e. 14th-15th July). Finally, this

290 leads to perform PMF over 16 variables and 849 time steps.

Since we combined data from 3 instruments presenting different measurement uncertainty calculation, signal-to-noise and relative number of variables, it is needed to ensure the well representativeness of each group in the PMF analysis (Tong et al., 2022). Some studies suggested to apply a relative instrument weight to balance the scaled residuals of each subgroup of data (Crippa et al., 2013; J. G. Slowik et al., 2010; Tong et al., 2022; Via et al., 2023). The details about this instrument weighting

295 process are given in the Supplement. As described in section 2.4.2, a cell-wise downweighting was applied to datapoints with a weak S2N ratio. PMF runs were performed from 1 to 12 factors to inspect and identify the most physically meaningful factors. 8 factors were clearly determined: biomass burning, cooking, industrial, dust resuspension, traffic, organic nitrate-rich (ON-rich), shipping and ammonium sulfate-rich (AS-rich) factors. However, conducting different seed runs showed a high degree of rotational ambiguity in the solution, with some unstable factors which cannot be resolved systematically (Table S4).

300 While it is common to set some variables to 0 in the factors profiles based on prior chemical knowledges of the sources (Bozzetti et al., 2017; Weber et al., 2019), this method did not allow a clear factors separation. Here, the entire profiles were constrained for the biomass burning, cooking and industrial factors using their profiles from the most interpretable solutions as base case. Profile constraints were applied with an a-value of 0.4, 0.1 and 0.05 for biomass burning, cooking and industrial, respectively, leading to a more stable solution.

305 Further discussions on the factor identification, the rotational ambiguity, the a-values selection for the constrained profiles and the acceptance criteria are provided in the Supplement section. Similarly to the two previous PMF analyses, a bootstrap analysis was conducted over 100 runs and all the accepted runs were averaged into the reported solution.

2.5 OP apportionment

An inversion method is applied on factors issued from all PMFs to assess contributions of the PM sources to the OP. The

310 dependent variable OP expressed in nmol.min^{-1}.m^{-3} is explained by a linear combination of mass contribution of PM sources (µg.m^{-3}) taken as independent variables as follows:

$$OP = H \times \beta_n + \varepsilon \qquad (6)$$

where OP vector (px1) is the measured OP (p observations) with 4h time-resolution, H is a matrix (nx(p+1)) of n sources resolved from the PMF analyses plus the intercept (data of the sources PMF with a time step of 1 h have been averaged over

the 4h time step of the OP data), and ε vector (px1) accounts for the misfit between the observations and the model. Regression coefficients β provided by the model (Eq. 6) are interpreted as intrinsic OP of the n sources (nmol.min^{-1}.µg^{-1}). Basically, it expresses how much the OP would increase if we increase 1 µg.m^{-3} of the given source. The source-specific OP contribution is calculated by multiplying the regression coefficient β of each source by the respective mass contribution of the source to PM. This methodology is essentially based on previous works detailed in Borlaza et al. (2021a) and Weber et al. (2021, 2018).

Three scenarii in the construction of the matrix H (Eq. 6), i.e. the contribution of various source factors of PM identified by each of the three PMFs, have been considered to make the best use of the results from the different PMFs. Three models were tested in each scenarii (e.g. 9 solutions): weighted least squares linear regression (WLS), weighted robust multiple linear regression with an iterative M-estimator, and partial least square regression (PLS). The description of both the three scenarii (Eq. S4, S5 and S6) and the three models (Eq. S7, S8 and S9) are shown in the Supplement. Best model solutions with the lowest RSR (RMSE standard deviation ratio) are presented: M-estimator in scenarios 1 and 2 (see Table S3) and WLS in scenario 3. Source factor contributions exhibiting a Pearson's association with OP less than 0.1 were discarded from the predictor variables. Finally, to provide robust estimates of model's output terms in scenario 3, the process was performed 500 times with bootstrapped inputs by following the method of Canonaco et al. (2021). Briefly, 15% of the input samples were randomly either removed or duplicated before each run. Output runs with $R^2_{adjusted}$ values below than the one found in the first inversion model without bootstrapping (Eq. 6) (i.e $R^2_{adjusted} < 0.3$ for OP$_{DTT}$ and $R^2_{adjusted} < 0.4$ for OP$_{AA}$ in scenario 3) were removed. Factors with a Variance Inflation Factor (VIF) > 10 were also removed, because it suggests strong collinearity between them (Calas et al., 2019). Robust linear regression was performed with the *MASS* package developed in R (Grange et al., 2022; Venables and Ripley, 1997) and weighted linear regression was performed using *stats* package developed in R.

3. Results

3.1 OP results

Meteorological conditions typical of those prevailing during summertime in the region happened during the period of the study, with land and sea breeze cycles (except between 20th and 24th July), associated with stable conditions characterized by ozone episodes (6 regulatory exceedances, with a maximum at 166 µg.m^{-3}). NO$_x$, O$_3$ and SO$_2$ average concentrations during OP apportionment period were respectively 20, 80, and 2.5 µg.m^{-3} (Fig. S5). The overall period (n = 83 samples) was characterized by an average PM$_1$ concentration of 13.2 ± 3.4 µg.m^{-3}.

This study is the first to characterise OP in France with a 4 h time step, allowing an overlook to the daily OP$_v$ variation. Figure 2a shows the difference between night and day and Fig. 2b presents the typical daily OP$_v$ variation (without firework episodes), associated with organic fraction of aerosol quantified by ToF-ACSM, metallic fraction of aerosol quantified by Xact, and PM$_1$ variations. The averages were calculated using 15 days during the period. Mass of PM$_1$, metallic elements organic aerosol and also OP$_{vDTT}$ are quite higher during the day than at night, while OP$_{vAA}$ has no significant variation between night and day. A t-test demonstrates no significant difference (p<0.05) between the OP$_v$ measured on the day (07:00 - 23:00 UTC) and the OP$_v$

measured at night (23:00 - 07:00 UTC), for both OP assays. Two ANOVA variance tests were separately performed on OP_{AA} and OP_{DTT} 4h series, and the result showed no significant difference between the two assays.

Figure S6b. presents the composition in major chemical components of PM_1 measured by ToF-ACSM, Xact and AE33 (organic
350   fraction, metallic fraction, NH_4^+, Cl^-, NO_3^-, SO_4^{2-}, BC_{FF} and BC_{WB}) , together with the comparison of the reconstructed mass with these chemical components and the PM_1 concentration measured with the FIDAS. The Spearman association between these 2 time series is $r_s = 0.47$, p <0.001. Figure S6a shows periods when the reconstructed mass fits well with the mass provided by the FIDAS, and periods when the reconstructed mass is overestimated and/or underestimated.

OP_{AA} and OP_{DTT} median values are respectively 0.62 nmol.min^{-1}.m^{-3} and 1.47 nmol.min^{-1}.m^{-3}. Figure 3 shows variations of
355   both OP assays set against PM_1 mass. These OP values are characteristic of the coastal environment in warm period (Calas et al., 2019), but we can note that they are rather low compared to many other series (for PM_{10} or $PM_{2.5}$) measured with the same methods in other environments (Weber et al., 2018).

Spearman correlation (rs) between PM_1 mass measured by FIDAS and, respectively, OP_{vAA} and OP_{VDTT} are 0.23 (p<0.01) and 0.63 (p<0.001). These values can be compared with those found in In 't Veld (2022) in Barcelona (urban metropolis with
360   industrial port, same typology of Marseille) on a 1-year study of PM_1. Spearman correlation (rs) between PM_1 mass and, respectively, OP_{vAA} and OP_{VDTT} are 0.29 (p<0.001) and 0.73 (p<0.001) in Barcelona. These values are close to those found in this study on the site of Marseille-Longchamp. In both cases, the association is much better for OP_{DTT} than for OP_{AA}.
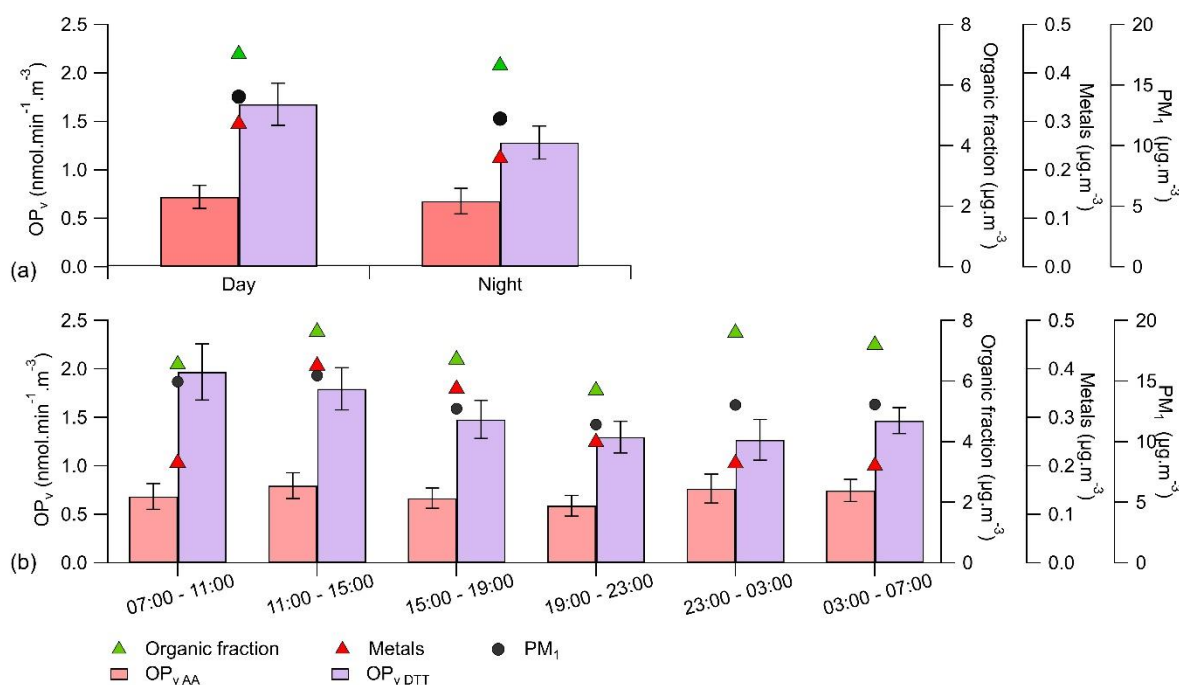
Figure 2. Profiles of $OP_{v\ AA}$, $OP_{v\ DTT}$, organic and metal fractions of submicron aerosol and PM_1 during **(a)** night (23:00 – 07:00) and day
365   (07:00 - 23:00 UTC) and **(b)** different times of the day following time step of OP (4h).
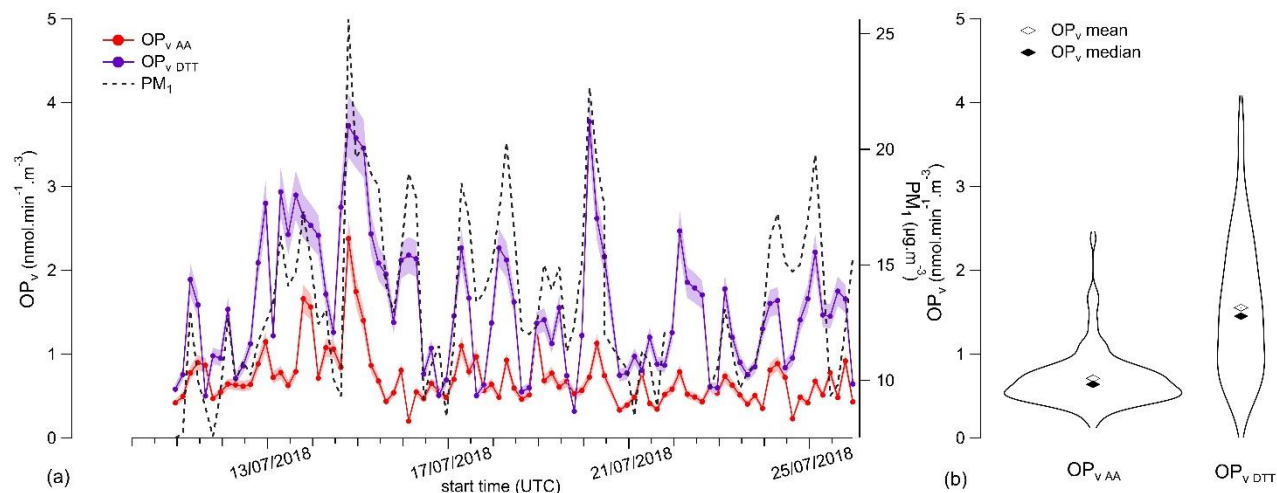
Figure 3. (a) $OP_{v\,AA}$, $OP_{v\,DTT}$ and PM_1 mass time series over the campaign in Marseille-Longchamp site. **(b)** Distribution of $OP_{v\,AA}$ and OP_{vDTT} in mean and median values.

3.2 Interpretation of PMF factors

3.2.1 PMF analysis of OA

The $PMF_{organics}$ results are presented in the supplement section with the profiles of the five factors (Fig. S7a), the time series (Fig. S7b), the relative fractions (Fig. S7c) and the diurnal cycles (Fig. S7d). As expected in this period, the secondary fraction including both LOOA and MOOA contributed to the highest part of OA with 33.4% each. HOA represented 16.3% of the total OA, followed by COA (13.7%) and Sh-IndOA (3.2%). HOA is assumed to be related to traffic exhaust emissions and displayed a distinct bimodal pattern with significant peaks during the morning and evening rush-hours. COA also showed a bimodal pattern with increased concentrations during the lunch time and the evening. Sh-IndOA concentrations accounted for combined plumes from the industrial area of Fos-sur-mer and from the shipping activity of Marseille harbour. These emissions are advected on site by sea breeze in the morning and slowly decreased through the day. LOOA and MOOA are distinguished based on their f44/f43 ratio, with the higher ratio for the more oxidized part. According to the diurnal cycles, MOOA showed a flat pattern suggesting a long-range transported origin and a slight increase at mid-day potentially attributed to more local photochemical activity. By contrast, LOOA concentrations were higher at night related to some night-time chemistry. Further OA sources descriptions in MRS-LCP are provided in Chazeau et al. (2022).

3.2.2 PMF analysis of metals

The PMF_{metals} solution is investigated with the factor profiles and time series in Fig. 4, the factor relative diurnal cycles and contributions are presented in Fig. S8. Non-parametric wind regressions (NWR) were also performed to determine the sources

concentrations attributed to their geographical origins using the wind direction and velocity (Henry et al., 2009; Petit et al., 2017). The results are displayed in Fig. S9.

Firework: This factor was only resolved for a short time from 13<rd> to 15<th> July (see section 2.4.2). Over its activity period, the
390   factor represented a major fraction of the total elements mass (up to 80%) and contributed to K (73%), Bi (100%), Ti (71%) and Cu (68%). These elements are usually found in fireworks composition (Manousakas et al., 2022; Perrino et al., 2011; Rai et al., 2020; Vecchi et al., 2008). K is both a component of gunpowder (Drewnick et al., 2006) and is used as oxidizer for firework bangs, while Cu and Ti are blue and white producers when ignited.
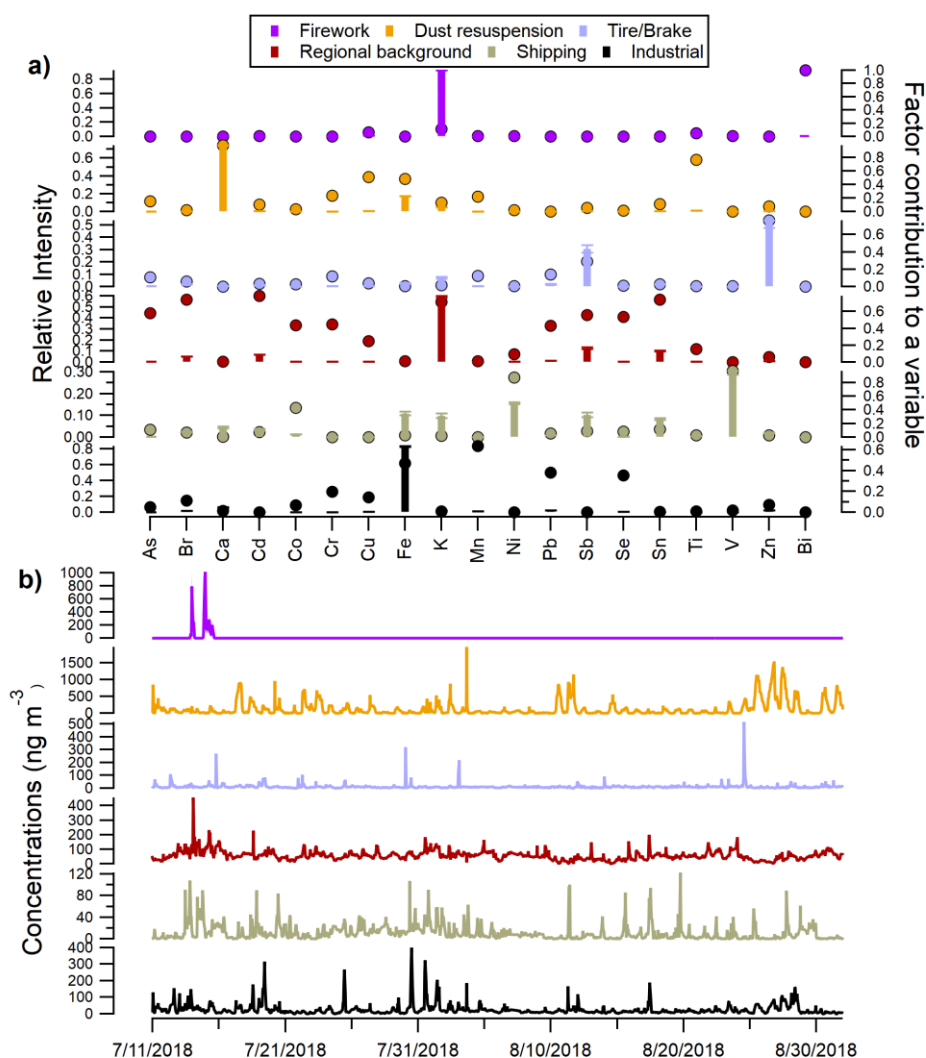
Figure 4. Average factor profiles **(a)** and time-series **(b)** for the 6 factors resolved by the PMF analysis.

Dust resuspension: This factor accounted for the largest contribution to the total elemental composition (53.7%). Its profile presented the main fraction to Ca (98%) and significant contributions to Ti (76%), Cu (51%) and Fe (48%). These elements are major constituents of crustal soils and can be considered here as urban dust (Almeida et al., 2020; Rai et al., 2021). Ca is also a compound often used for construction materials (Manousakas et al. 2022). The public construction influence is supported

400 by the factor diurnal profile which displayed increasing concentrations at 07h00 UTC followed by stable levels during the day and very low concentrations at night. The NWR plot showed a clear geographical origin from the north-west associated with a strong wind. Dust resuspension might occur under the "Mistral" conditions (a regional wind for the Rhone Valley) with enhanced concentrations under high velocity wind and dry conditions (Fig. S11). The factor could also include resuspension from non-exhaust traffic emissions due to the significant contribution of Cu.

405 *Tire/Brake wear:* This factor showed high contributions to Zn (76%) and Sb (29%). The factor diurnal profile didn't exhibit a distinct pattern and the time series were often affected by some spikes (Fig. 4b) which can be attributed to local short events. The factor time series showed moderate correlation with exhaust traffic proxies such as BC_{FF} (r = 0.33). However, Zn and Sb elements are known tracers of the brake wear emissions (Grigoratos et Martini 2015; and references therein). While Zn is one of the most abundant metals in the brake linings, Sb is contained in the form of stibnite ($Sb2S3$) and employed as a lubricant

410 to reduce vibration (Roubicek et al., 2008). Moreover, Zn is considered as a marker of tire wear particles (Panko, Kreider, et Unice 2018). It has to be noted that the tire/brake wear factor contributes in a low extent to the total metal composition (5.3%). In a previous study in Zurich, Bukowiecki et al. (2009) showed that the contribution to non-exhaust emissions from both light and heavy-duty vehicles was very low in the submicrometer mode.

Regional background: This factor contributed to a large range of elements: K (71%), Cd (78%), Br (74%), Sn (74%) and to

415 some extent to As (58%), Sb (56%), Se (54%) and Pb (43%). The factor diurnal profile was mostly flat suggesting long-range transport of aged background compounds. This is supported by a strong correlation with the MOOA factor (r = 0.6) resolved during the $PMF_{organics}$ analysis. Furthermore, the NWR analysis displayed a regional geographical origin, with enhanced concentrations from the southerly sector (the Mediterranean Sea) and from the north-east sector with land breeze advecting aged air masses back to the site.

420 *Shipping and industrial:* Shipping factor accounted for the main fractions of V (97%), Ni (88%) and Co (43%). The V/Ni ratio was often suggested as a proxy of heavy fuel combustion (Pandolfi et al., 2011; Viana et al., 2014). Here, we found a ratio of ~2 which is in agreement with the typical range for shipping emissions (between 2 and 4) and with a ratio found in a previous study in Marseille (2.35; Salameh et al.). The industrial factor contributed to Fe (47%), Mn (63%), Pb (38%) and Se (35%). This factor profile showed similarities with profiles from several industrial areas (Fig. S15). The contributions of some major

425 elements (i.e. Fe, Ca, Mn, As, Zn) to the factor were in the same range than those of two iron converter and two storage zones measured by ICP-MS for the $PM_{2.5}$ fraction (Sylvestre et al., 2017). Combining these two factors (Shipping and industrial) showed a strong correlation (r = 0.74) and a similar diurnal pattern with Sh-IndOA (Fig. S16), which accounted for both the industrial emissions from Fos-sur-mer and the shipping activity from the harbour (Chazeau et al., 2022). The shipping diurnal profile in Fig. S8b displayed a bimodal pattern which is linked to the diurnal trend of the ships departures/arrivals at the harbour

430   (Chazeau et al., 2021). Once the sea breeze sets in, a first peak related to the ship arrivals is observed, followed by a second
peak at 17h00 UTC due to ships departures. The diurnal profile of the industrial factor also exhibits increasing concentrations
once the sea breeze occurs, which then gradually decrease through the day. The NWR analyses support that industrial and
shipping factors were advected onsite by breeze from the Mediterranean Sea as they revealed clear hotspots from the south-
westerly sector. Shipping factor showed high concentrations at lower wind speed than for the industrial factor, highlighting
435   more local emissions that were expected due to the proximity of the harbour.

3.2.3 PMF analysis of PM$_1$

The full PM$_1$ source apportionment solution is explored in this section with the average factor profiles (Fig. 5a), the time series
(Fig. 5b), the pie chart of mass contributions (Fig. 5c) and the average diurnal profiles (Fig. 5d). The comparison of the time
series over the OP sample period of these factor profiles with those of the two OP assays (OP$_{AA}$ and OP$_{DTT}$) is shown on Fig. 6.
440   Biomass burning highly contributed to BC$_{WB}$ (81%) and to a lower extent to regional background metals (32%) and MOOA
(18%). The factor accounted for 5.1% of the total PM$_1$ concentration. While no primary biomass burning organic aerosol
(BBOA) factor was resolved with the PMF$_{organics}$ analysis in summer, the presence of a significant MOOA contribution reflects
the influence of secondary process in this biomass burning factor. The low concentrations of this factor is in agreement with
minor regional emissions linked to agricultural activities, wildfires and cooking practices such as BBQ, transformed through
445   oxidation processes during regional transport and aging (Chazeau et al., 2022; Cubison et al. 2011).

Cooking mainly includes contribution to COA (92%) and MOOA (34%) and represented 14.2% to the total PM$_1$ mass. Even
if its diurnal pattern is similar to the one from primary COA, the factor is mixed with a secondary organic aerosol fraction.
Moreover, the cooking source included an unexpected contribution to Cl$^-$ (19%), which was already observed in a rural
environment in Po Valley (Dall'Osto et al., 2015). While this study showed high contributions of Cl$^-$ and oxygenated organic
450   aerosol with COA in the cooking source that may be associated to some additional emissions from agricultural activities and
waste disposal, these sources are not expected at our urban site.

As expected, the industrial factor was characterized by high contributions to industrial metals (74%) and Sh-IndOA (46%).
The factor contributes little to the PM$_1$ composition (3.2%). Similar contributions were found in another Mediterranean coastal
city, Barcelona (4%; Via et al., 2023), and in some French urban sites (Weber et al., 2019).
455   The dust resuspension factor was exclusively driven by metals and presented some identical features with the dust resuspension
factor from the PMF$_{metals}$ (100% of the variable). It has to be noted that the factor included also some weak contributions to the
brake/tire wear and industrial metals (~10% each) which can be affected by the resuspensions processes.

Traffic source was mostly composed of HOA (32%), BC$_{FF}$ (44%) and to a lesser extent of LOOA (15%), and showed also a
large contribution of these variables (83%, 79% and 18%, respectively). Tire/brake wear metals were also important
460   contributors to this factor (29% of the total variable). However, this component presented the highest unexplained variation
(>30%) from all the dataset (Fig. S14) and revealed some over splitting in several factors. It should be emphasized that 23%
of the traffic source was constituted of SOA (LOOA and MOOA) meaning that primary traffic contribution is mixed with

secondary aerosol concentrations attributed to fast oxidation of freshly emitted particles (Chirico et al., 2011). The factor represented the second highest fraction of the PM$_1$ mass (21.4%).

465
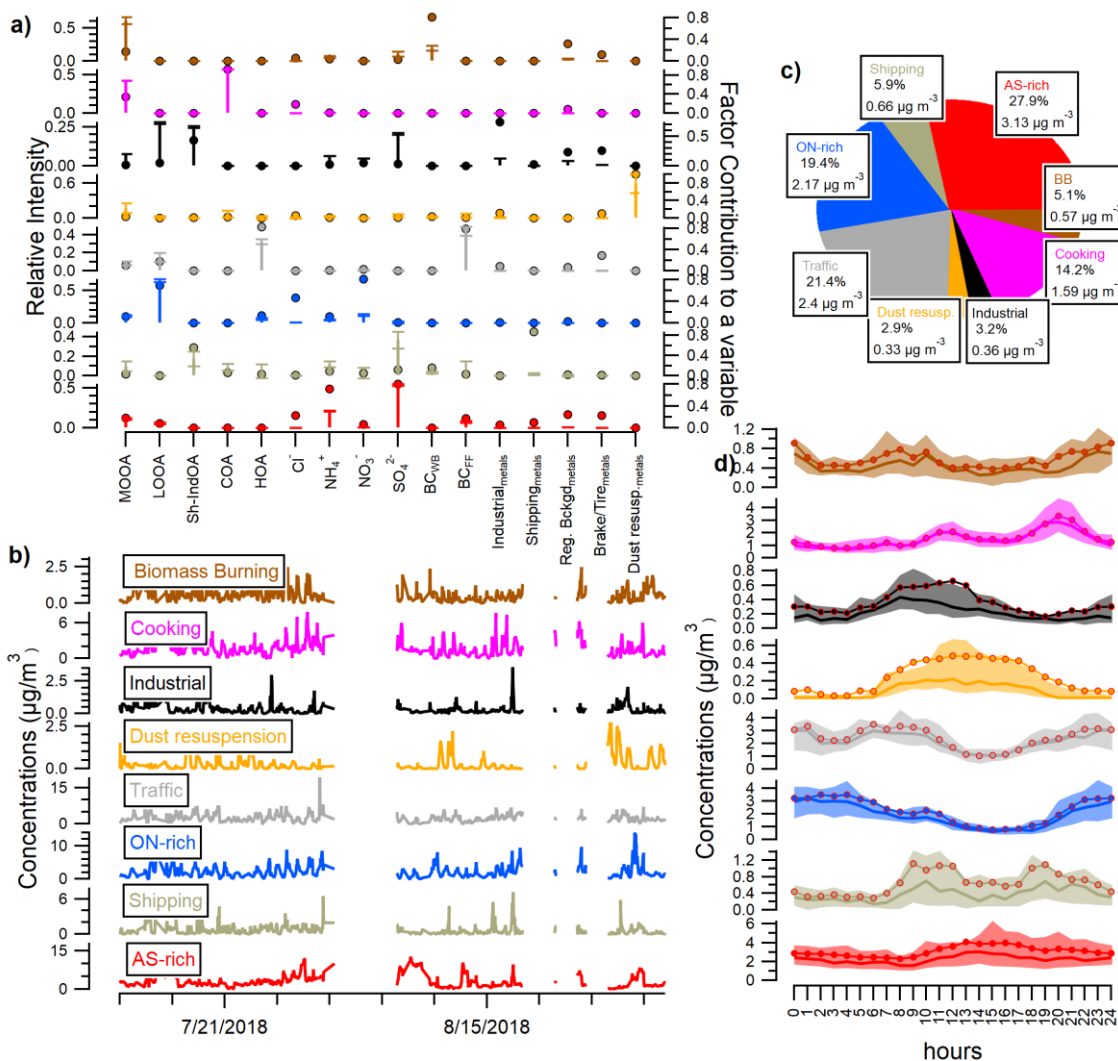
Figure 5. Average factor profiles **(a)**, time-series **(b)**, pie chart contributions **(c)** and diurnal cycles (solid lines indicate the median, red circles the mean and shaded areas the 25th-75th percentile range) **(d)** for the 8 factors from the PMF$_{PM1}$ solution.

470   The organic nitrate-rich (ON-rich) factor was resolved based on the high contribution to NO$_3^-$ (81%) and LOOA (69%). This factor accounted for 19.4% of the PM$_1$. The diurnal trend of this factor suggested contributions from night-time chemistry. A significant pathway might be the oxidation of biogenic VOCs by NO$_3$ radicals to produce organic nitrate particles (Kiendler-Scharr et al., 2016; Xu et al., 2015).

The shipping source showed expected contribution from shipping metals (87%) and Sh-IndOA (56%) and accounted for 5.9%
475 of the PM_1. Shipping emissions from the Marseille harbour are further described in the section 3.3.2.

The AS-rich factor represented the largest fraction of the PM_1 (27.9%) and was dominated by ammonium sulfate contribution
(80% of SO_4^{2-} and 72% of NH_4^+). SO_4^{2-}/NH_4^+ ratio in this profile was 2.57, which is consistent with the mass ratio of
ammonium sulfate in the $(NH_4)_2SO_4$ form (2.66). The remaining fraction of SO_4^{2-} was attributed to the shipping (12%) and
industrial (4%) factors. The diurnal profile of AS-rich showed enhanced concentrations in the afternoon linked to the
480 photochemical production of sulfate from its precursor SO_2 (Zhuang et al., 1999). The presence of SOA contribution in this
factor (16%) suggests its formation by similar process (i.e. photooxidation) (Bozzetti et al., 2017; Salameh et al., 2018; Waked
et al., 2014). This ammonium sulfate pattern was already pointed out in summer in Marseille and was attributed to mixed
Mediterranean sulfate sources (including industrial and shipping emissions) from regional origin transported by processed air
masses (Chazeau et al., 2021). It should be noted that AS-rich factor might also include some other anthropogenic influence
485 due to its moderate composition of BC_{FF} (17%).

Overall, this PMF approach successfully resolved the several sources of PM_1 in Marseille which have already been highlighted
in other studies (Bozzetti et al., (2017); El Haddad et al., 2013) with AMS data; Chazeau et al. (2022) with ToF-
ACSM data; Salameh et al., (2018) with $PM_{2.5}$ offline filters). The results bring new insights on the source apportionment of
the site, in particular with a distinct separation between the industrial and shipping emissions advected simultaneously onsite,
490 and also the resolution of ON-rich factor which have not been resolved before.
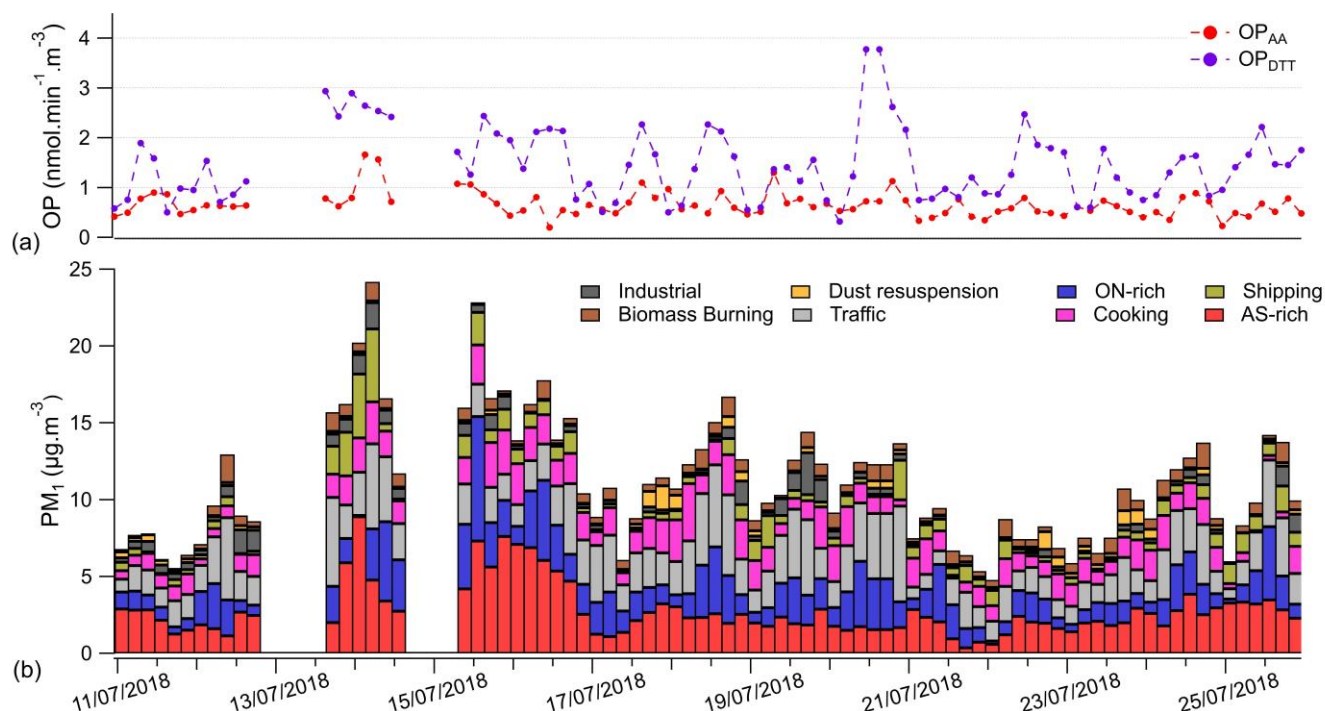
Figure 6 (a) Time series of both OP assays during OP sampling campaign; **(b)** Contribution of source factors provided by the PMF_{PM1} to PM_1 over time.

3.3 Results of OP's inversion for the PMF_{PM1} sources

Associations between each of the sources provided by the PMF_{PM1} and the OP measurements are shown in Table S5. The observation of these direct correlations shows that none of the sources identified is dominant on its own in explaining the changes in both OP assays. It is the combination of sources that ultimately leads to the observed OP_{AA} and OP_{DTT}.

3.3.1 Models accuracy

M-estimator inversion model's results issued from $PMF_{organics}$ (scenario 1) or PMF_{metals} (scenario 2) alone are respectively presented in Table S3a and Table S3b, and are discussed in supplementary information. The results obtained with WLS inversion applied to the PMF_{PM1} (scenario 3) are the most robust and sounded on geochemical base. Cooking source factor was not considered based on its anti-correlation with OP_{vAA}. All other source factors included in the PMF_{PM1} were considered since they did not show any multicollinearity (VIF<5). Accuracy of this model was estimated by its robustness (validity of error's model generated by the bootstrap method) and by a residual analysis between OP observed and OP reconstructed by the model. Breusch-Pagan test performed for each assay assess the absence of heteroscedasticity in model's residuals ($p < 10^{-5}$) (see Fig. S17). Observed OP and reconstructed OP fairly correlate for both assays (OP_{vAA}: r = 0.44, $R^2_{adjusted}$ = 0.4 - OP_{vDTT}: r = 0.54, $R^2_{adjusted}$ = 0.3, p < 0.001 in both cases).

3.3.2 Intrinsic OP$_{DTT}$ and OP$_{AA}$

510 Intrinsic OP (i.e β coefficients provided by WLS regression models in scenario 3 (see 2.5), thereafter denoted OP$_m$) of source factor contributions identified by PMF$_{PM1}$ are shown in Table 1 and are discussed below.

Dust resuspension and Industrial are the main reactive sources towards ascorbic acid assay, with OP$_{mAA}$ mean values of 0.26 $\pm$ 0.03 and 0.22 $\pm$ 0.05 nmol.min^{-1}.µg^{-1} respectively. Since 51 % of copper is found in the dust resuspension factor and as various metals (Fe, Cr, Ti, Mn, Pb or Se) were found in these two factors, ascorbic acid assay confirms its metal-sensitivity

515 especially towards Cu (Daellenbach et al., 2020; Grange et al., 2022; Pant et al., 2015; Pant and Harrison, 2013). In parallel, Calas et al. (2019) and Gao et al. (2020) pointed the role of organic species in OP$_{AA}$ response, which is in this study sensitive to both less and more oxidized organic aerosols (LOOA and MOOA factors from the PMF$_{organics}$) and organic compounds from harbour and plant activities (Sh-IndOA factor also from the PMF$_{organics}$). Thus, 27% and 25% of industrial source factor is constituted by LOOA and Sh-IndOA factors respectively, and 17% of dust resuspension source factor is constituted by MOOA

520 factor. As already reported in Weber et al. (2019) on the OP apportionment study on PM$_{10}$ in the same site, DTT appears to be sensitive to a wide range of sources. In this study, AS-rich, shipping and biomass burning sources are the main drivers of OP$_{DTT}$ with respectively OP$_{mDTT}$ values of 0.18 $\pm$ 0.02 nmol.min^{-1}.µg^{-1}, 0.16 $\pm$ 0.03 nmol.min^{-1}.µg^{-1} and 0.15 $\pm$ 0.06 nmol.min^{-1}.µg^{-1}.

In addition to the inherent reactivity of the chemical species, high levels of SO$_4^{2-}$ in AS-rich and shipping sources (respectively

525 54% and 36% of the source factor) may increase OP activity through the dissolution of some metallic elements under acidic conditions (Fang et al., 2017). In a same way, toxicological studies highlighted the role of BC$_{WB}$ (81% of the quantification of BC$_{WB}$ is founded in biomass burning source) as an indicator of co-transported high DTT-reactive species like metals or quinones (Niranjan and Thakur, 2017; Shang et al., 2016).

Although several studies emphasized the role of road traffic in OP (Daellenbach et al., 2020; Fang et al., 2016; Saffari et al.,

530 2015), OP$_m$ of the traffic source is surprisingly very low for both OP assays in our case (OP$_{mAA}$: 0.01 $\pm$ 0.02 nmol.min^{-1}.µg^{-1} - OP$_{mDTT}$ = 0.02 $\pm$ 0.02 nmol.min^{-1}.µg^{-1}). This result might be explained by the fact that non-exhaust traffic emissions traditionnally associated to OP are mainly found in a coarser mode than PM$_1$ (Piscitello et al., 2021).

Interestingly, the traffic source is well correlated to OP$_{vAA}$ and OP$_{vDTT}$ (r = 0.40 – r = 0.34, p < 0.01) but associated to the lowest OP$_m$ values. Although Pearson's correlation between OP values and source factor contributions is a first indication of

535 the OP sensitivity towards certain sources, it is likely preferable to be used in association with an MLR-like model, as already underlined by Weber et al. (2018) and In 't Veld (2022).

540

Table 1. Intrinsic OP_{AA} and OP_{DTT} (OP_m) expressed in nmol.min^{-1}.µg^{-1} of sources provided by PMF_{PM1} method over the OP sampling campaign without fireworks episode (n = 78 samples) for both OP assays. Values are the mean ± standard deviation from selected bootstraps of the optimal solution.

	Intercept	BB	Cooking	Industrial	Dust resuspension	Traffic	ON-rich	Shipping	AS-rich
	nmol.min^{-1}.m^{-3}			nmol.min^{-1}.µg^{-1}					
OP_{AA}	0.38±0.03	0.01±0.04	-0.01±0.02	0.22±0.05	0.26±0.03	0.01±0.02	0.03±0.01	0.04±0.02	-0.02±0.02
OP_{DTT}	0.45±0.05	0.15±0.06	n.c.	0.04±0.04	-0.05±0.03	0.02±0.02	0.06±0.02	0.16±0.03	0.18±0.02

3.3.3 Population exposure: median contribution of OP

Source-specific contributions to OP_{AA}, OP_{DTT}, and PM_1 mass are presented below, ranked in decreasing order and reported as median value in Fig. 7. The same results gathered in mean values are shown in Fig. S18. These two metrics do not address the same issue: mean value is generally used in the atmospheric community while epidemiological studies prefer to rely on median value, excluding outlier events which are not representative of a chronic exposure of the population. We observe little difference in the ranking of sources between mean and median values due to the overall low variability of observed OP during the sampling campaign. However, the mean value and the median value of AS-rich source factor contribution to OP_{DTT} are significantly different, with mean value being four times higher than the median value. The median values of AS-rich source contribution stay close to those of biomass burning, shipping and ON-rich source factor contributions (respectively with OP_{vDTT} values of 0.1 ± 0.01 nmol.min^{-1}.m^{-3}, 0.09 ± 0.01 nmol.min^{-1}.m^{-3}, 0.08 ± 0.01 nmol.min^{-1}.m^{-3}, 0.08 ± 0.02 nmol.min^{-1}.m^{-3}).

As already observed in other studies (Borlaza et al., 2021a; Weber et al., 2021, 2018), the main observation in Fig. 7 is the clear difference in the factor source contributions when considering OP activity or PM_1 mass. This highlights that the sources driving OP activity are not the same as the ones driving PM mass. While the industrial source contributes little to the PM_1 mass (0.26 µg.m^{-3}), it has the highest OP_{vAA} value (0.06 ± 0.01 nmol.min^{-1}.m^{-3}) with ON-rich factor (0.05 ± 0.02 nmol.min^{-1}.m^{-3}) and followed by dust resuspension (0.04 ± 0.00 nmol.min^{-1}.m^{-3}) source. In the same way, shipping and biomass burning sources highly contribute to OP_{vDTT} (0.08 ± 0.03 and 0.09 ± 0.02 nmol.min^{-1}.m^{-3}) while each source contributes less than 13% of PM_1 total mass. On the contrary, AS-rich and cooking sources display negative contributions to OP_{vAA} while they contribute significantly to the PM_1 mass. The traffic source does not appear to be a main driver in both type of OP although its high PM_1 mass contribution (21.4%). However, we must note a very large standard deviation in the contribution of this factor to OP_{vDTT}.

A previous study was conducted over a year on PM_{10} in Marseille-Longchamp site, and already emphasizes the contribution of biomass burning and Heavy Fuel Oil (HFO; related to shipping activity) to $OP_{vAA,}$ and OP_{vDTT}. Even if similar results can be found, they should be treated with caution as different fractions of PM are being studied.

Even though OA and metals are found in all sources, the results suggest that only a fraction of these compounds have a
570 substantial impact on OP activity of PM_1. Overall, this draws our attention to the contribution of multiple sources (local and
regional) with low PM_1 mass loading in the chronic exposure of PM pollutant.
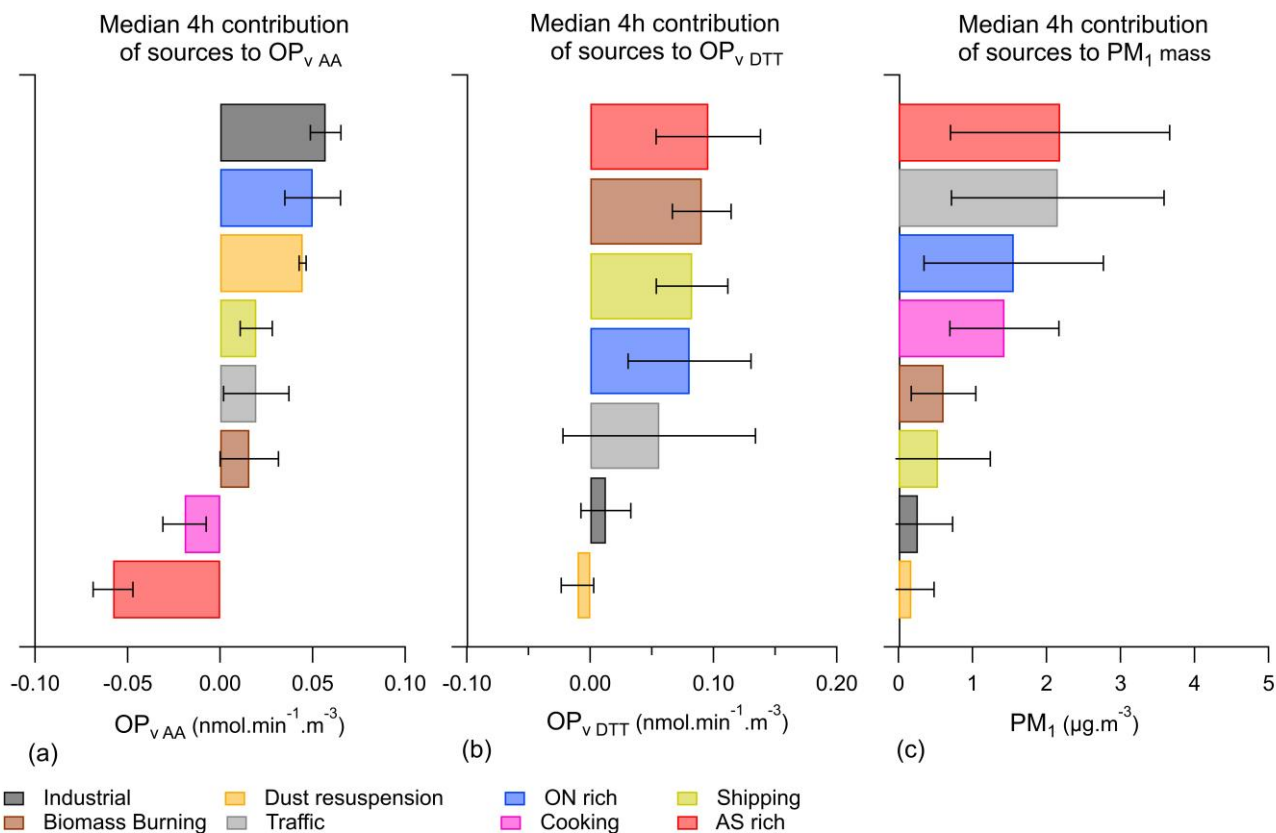
Figure 7. Median contribution of the sources identified by PMF_{PM1} over the OP sampling campaign without fireworks episode (n = 78
575 samples) to **(a)** $OP_{v\,AA}$, **(b)** $OP_{v\,DTT}$, **(c)** PM_1. Error bars represents the standard deviation of the data distribution

4. Limits of the study

The robust method used in this study is promising for further practical applications. However, we can bring some limitations
that can explain the moderate OP reconstruction. Mainly, little variability in OP measurements and in chemical composition
580 was observed at the Marseille Longchamp site over a 15 day period, implying difficulties for models such as MLR to accurately
reconstruct OP peaks and thus lowers Pearson correlation coefficient r between observed OP and modelled OP. Then,
averaging the online data which have a time step of 15 min and 1 h respectively for ToF-ACSM and Xact over the time step
of the OP (4 h) led to a levelling of the pollution peaks visible on the online analysers. Also, times series of OP and chemistry
originates from offline and online methodologies that may introduce additional uncertainties to the results of the study, related

585 to some extent of sampling artefact. Furthermore, recent studies suspected non-linear relationships for the source apportionment of OP, especially when increasing of PM mass (Calas et al., 2017; Charrier et al., 2016; Grange et al., 2022; Weber et al., 2021). Another main limitation is the lack of data between 12 July 2018 21:00 – 13 July 2018 05:00 UTC (3 points) and 14 July 2018 17:00 – 15 July 2018 05:00 UTC (4 points), resulting in difficulty for the model to reconstitute certain OP peaks. Lastly, the propagation of uncertainties can be a limitation as we increase the imprecision of the actual measured

590 OP. The combination of all these limits could explain the unrecovered percentage of the OP's variance by the model (i.e. intercept).

5. Conclusions

To the best of our knowledge, this study is the first to apportion OP from sources provided by a two-step PMF approach using high time resolution online Xact and ToF-ACSM data. It also provides additional knowledge on OP of PM_1 which is still little

595 studied although the major role of the submicronic fraction of the aerosol in public health concerns is generally highlighted. A redistribution of the sources between mass and OP contributions was observed in both OP_{AA} and OP_{DTT} assays, highlighting the limiting capacity of the mass concentration alone in understanding the redox activity of PM. While the PM_1 mass concentrations were dominated by AS-rich, traffic and ON-rich sources, factors with an anthropogenic origin such as industries, shipping, biomass burning and dust resuspension, represented only a few percent. However, these factors with a

600 low mass concentration showed a high OP contribution. As a consequence, making effort in reducing these specific anthropogenic sources, regardless the PM mass regulations, might result in a significant reduction of OP in the submicronic mode.

We demonstrated that OP apportionment models performed on source factors deconvolved from partial aerosol composition (only metals or organics) are not robust. The two-step PMF^2 approach appears as a substantial method to integrate a wider

605 range of markers (organic and inorganic) for a better identification of PM sources. The OP apportionment via a WLS inversion model led to comprehensive and realistic OP sources.

Several improvements can be suggested to address the limitations mentioned in Section 4, as subsequently introduce source uncertainties from PMF model into OP deconvolution model. Furthermore, these findings pave the way of coupling recent

610 prototypes allowing in-situ OP data with online chemical analysers aiming to understand short-lived processes.

Competing interests

The contact author has declared that none of the authors has any competing interests.

References

Abrams, J. Y., Weber, R. J., Klein, M., Samat, S. E., Chang, H. H., Strickland, M. J., Verma, V., Fang, T., Bates, J. T., Mulholland, J. A., Russell, A. G., and Tolbert, P. E.: Associations between Ambient Fine Particulate Oxidative Potential and Cardiorespiratory Emergency Department Visits, Environ Health Perspect, 125, https://doi.org/10.1289/EHP1545, 2017.

Äijälä, M., Daellenbach, K. R., Canonaco, F., Heikkinen, L., Junninen, H., Petäjä, T., Kulmala, M., Prévôt, A. S. H., and Ehn, M.: Constructing a data-driven receptor model for organic and inorganic aerosol – a synthesis analysis of eight mass spectrometric data sets from a boreal forest site, Atmos. Chem. Phys., 19, 3645–3672, https://doi.org/10.5194/acp-19-3645-2019, 2019.

Almeida, S. M., Manousakas, M., Diapouli, E., Kertesz, Z., Samek, L., Hristova, E., Šega, K., Alvarez, R. P., Belis, C. A., and Eleftheriadis, K.: Ambient particulate matter source apportionment using receptor modelling in European and Central Asia urban areas, Environmental Pollution, 266, 115199, https://doi.org/10.1016/j.envpol.2020.115199, 2020.

Ayres, J. G., Borm, P., Cassee, F. R., Castranova, V., Donaldson, K., Ghio, A., Harrison, R. M., Hider, R., Kelly, F., Kooter, I. M., Marano, F., Maynard, R. L., Mudway, I., Nel, A., Sioutas, C., Smith, S., Baeza-Squiban, A., Cho, A., Duggan, S., and Froines, J.: Evaluating the Toxicity of Airborne Particulate Matter and Nanoparticles by Measuring Oxidative Stress Potential—A Workshop Report and Consensus Statement, Inhalation Toxicology, 20, 75–99, https://doi.org/10.1080/08958370701665517, 2008.

Beelen, R., Raaschou-Nielsen, O., Stafoggia, M., Andersen, Z. J., Weinmayr, G., Hoffmann, B., Wolf, K., Samoli, E., Fischer, P., Nieuwenhuijsen, M., Vineis, P., Xun, W. W., Katsouyanni, K., Dimakopoulou, K., Oudin, A., Forsberg, B., Modig, L., Havulinna, A. S., Lanki, T., Turunen, A., Oftedal, B., Nystad, W., Nafstad, P., De Faire, U., Pedersen, N. L., Östenson, C.-G., Fratiglioni, L., Penell, J., Korek, M., Pershagen, G., Eriksen, K. T., Overvad, K., Ellermann, T., Eeftens, M., Peeters, P. H., Meliefste, K., Wang, M., Bueno-de-Mesquita, B., Sugiri, D., Krämer, U., Heinrich, J., de Hoogh, K., Key, T., Peters, A., Hampel, R., Concin, H., Nagel, G., Ineichen, A., Schaffner, E., Probst-Hensch, N., Künzli, N., Schindler, C., Schikowski, T., Adam, M., Phuleria, H., Vilier, A., Clavel-Chapelon, F., Declercq, C., Grioni, S., Krogh, V., Tsai, M.-Y., Ricceri, F., Sacerdote, C., Galassi, C., Migliore, E., Ranzi, A., Cesaroni, G., Badaloni, C., Forastiere, F., Tamayo, I., Amiano, P., Dorronsoro, M., Katsoulis, M., Trichopoulou, A., Brunekreef, B., and Hoek, G.: Effects of long-term exposure to air pollution on natural-cause mortality: an analysis of 22 European cohorts within the multicentre ESCAPE project, The Lancet, 383, 785–795, https://doi.org/10.1016/S0140-6736(13)62158-3, 2014.

Belis, C. A., Pikridas, M., Lucarelli, F., Petralia, E., Cavalli, F., Calzolai, G., Berico, M., and Sciare, J.: Source apportionment of fine PM by combining high time resolution organic and inorganic chemical composition datasets, Atmospheric Environment: X, 3, 100046, https://doi.org/10.1016/j.aeaoa.2019.100046, 2019.

Boogaard, H., Janssen, N. A. H., Fischer, P. H., Kos, G. P. A., Weijers, E. P., Cassee, F. R., van der Zee, S. C., de Hartog, J. J., Brunekreef, B., and Hoek, G.: Contrasts in Oxidative Potential and Other Particulate Matter Characteristics Collected Near Major Streets and Background Locations, Environmental Health Perspectives, 120, 185–191, https://doi.org/10.1289/ehp.1103667, 2012.

Borlaza, L. J., Weber, S., Marsal, A., Uzu, G., Jacob, V., Besombes, J.-L., Chatain, M., Conil, S., and Jaffrezo, J.-L.: 9-year trends of PM10 sources and oxidative potential in a rural background site in France, Aerosols/Field Measurements/Troposphere/Chemistry (chemical composition and reactions), https://doi.org/10.5194/acp-2021-839, 2021a.

Borlaza, L. J. S., Cosep, E. M. R., Kim, S., Lee, K., Joo, H., Park, M., Bate, D., Cayetano, M. G., and Park, K.: Oxidative potential of fine ambient particles in various environments, Environmental Pollution, 243, 1679–1688, https://doi.org/10.1016/j.envpol.2018.09.074, 2018.

Borlaza, L. J. S., Weber, S., Jaffrezo, J.-L., Houdier, S., Slama, R., Rieux, C., Albinet, A., Micallef, S., Trébluchon, C., and Uzu, G.: Disparities in particulate matter (PM10) origins and oxidative potential at a city scale (Grenoble, France) – Part 2:

655 Sources of PM10 oxidative potential using multiple linear regression analysis and the predictive applicability of multilayer perceptron neural network analysis, Atmos. Chem. Phys., 21, 9719–9739, https://doi.org/10.5194/acp-21-9719-2021, 2021b.

Bozzetti, C., Sosedova, Y., Xiao, M., Daellenbach, K. R., Ulevicius, V., Dudoitis, V., Mordas, G., Byčenkienė, S., Plauškaitė, K., Vlachou, A., Golly, B., Chazeau, B., Besombes, J.-L., Baltensperger, U., Jaffrezo, J.-L., Slowik, J. G., El Haddad, I., and Prévôt, A. S. H.: Argon offline-AMS source apportionment of organic aerosol over yearly cycles for an urban, rural, and

660 marine site in northern Europe, Atmos. Chem. Phys., 17, 117–141, https://doi.org/10.5194/acp-17-117-2017, 2017a.

Bozzetti, C., El Haddad, I., Salameh, D., Daellenbach, K. R., Fermo, P., Gonzalez, R., Minguillón, M. C., Iinuma, Y., Poulain, L., Elser, M., Müller, E., Slowik, J. G., Jaffrezo, J.-L., Baltensperger, U., Marchand, N., and Prévôt, A. S. H.: Organic aerosol source apportionment by offline-AMS over a full year in Marseille, Atmos. Chem. Phys., 17, 8247–8268, https://doi.org/10.5194/acp-17-8247-2017, 2017b.

665 Bozzetti, C., El Haddad, I., Salameh, D., Daellenbach, K. R., Fermo, P., Gonzalez, R., Minguillón, M. C., Iinuma, Y., Poulain, L., Elser, M., Müller, E., Slowik, J. G., Jaffrezo, J.-L., Baltensperger, U., Marchand, N., and Prévôt, A. S. H.: Organic aerosol source apportionment by offline-AMS over a full year in Marseille, Atmospheric Chemistry and Physics, 17, 8247–8268, https://doi.org/10.5194/acp-17-8247-2017, 2017c.

Bukowiecki, N., Lienemann, P., Hill, M., Figi, R., Richard, A., Furger, M., Rickers, K., Falkenberg, G., Zhao, Y., Cliff, S. S.,

670 Prevot, A. S. H., Baltensperger, U., Buchmann, B., and Gehrig, R.: Real-World Emission Factors for Antimony and Other Brake Wear Related Trace Elements: Size-Segregated Values for Light and Heavy Duty Vehicles, Environ. Sci. Technol., 43, 8072–8078, https://doi.org/10.1021/es9006096, 2009.

Calas, A., Uzu, G., Martins, J. M. F., Voisin, D., Spadini, L., Lacroix, T., and Jaffrezo, J.-L.: The importance of simulated lung fluid (SLF) extractions for a more relevant evaluation of the oxidative potential of particulate matter, Sci Rep, 7, 11617,

675 https://doi.org/10.1038/s41598-017-11979-3, 2017.

Calas, A., Uzu, G., Kelly, F. J., Houdier, S., Martins, J. M. F., Thomas, F., Molton, F., Charron, A., Dunster, C., Oliete, A., Jacob, V., Besombes, J.-L., Chevrier, F., and Jaffrezo, J.-L.: Comparison between five acellular oxidative potential measurement assays performed with detailed chemistry on PM10 samples from the city of Chamonix (France), Atmos. Chem. Phys., 18, 7863–7875, https://doi.org/10.5194/acp-18-7863-2018, 2018.

680 Calas, A., Uzu, G., Besombes, J.-L., Martins, J. M. F., Redaelli, M., Weber, S., Charron, A., Albinet, A., Chevrier, F., Brulfert, G., Mesbah, B., Favez, O., and Jaffrezo, J.-L.: Seasonal Variations and Chemical Predictors of Oxidative Potential (OP) of Particulate Matter (PM), for Seven Urban French Sites, Atmosphere, 10, 698, https://doi.org/10.3390/atmos10110698, 2019.

Canonaco, F., Crippa, M., Slowik, J. G., Baltensperger, U., and Prévôt, A. S. H.: SoFi, an IGOR-based interface for the efficient use of the generalized multilinear engine (ME-2) for the source apportionment: ME-2 application to aerosol mass spectrometer

685 data, Atmos. Meas. Tech., 6, 3649–3661, https://doi.org/10.5194/amt-6-3649-2013, 2013.

Canonaco, F., Tobler, A., Chen, G., Sosedova, Y., Slowik, J. G., Bozzetti, C., Daellenbach, K. R., El Haddad, I., Crippa, M., Huang, R.-J., Furger, M., Baltensperger, U., and Prévôt, A. S. H.: A new method for long-term source apportionment with time-dependent factor profiles and uncertainty assessment using SoFi Pro: application to 1 year of organic aerosol data, Atmos. Meas. Tech., 14, 923–943, https://doi.org/10.5194/amt-14-923-2021, 2021.

690 Charrier, J. G., McFall, A. S., Vu, K. K.-T., Baroi, J., Olea, C., Hasson, A., and Anastasio, C.: A bias in the "mass-normalized" DTT response – An effect of non-linear concentration-response curves for copper and manganese, Atmospheric Environment, 144, 325–334, https://doi.org/10.1016/j.atmosenv.2016.08.071, 2016.

Chazeau, B., Temime-Roussel, B., Gille, G., Mesbah, B., D'Anna, B., Wortham, H., and Marchand, N.: Measurement report: Fourteen months of real-time characterisation of the submicronic aerosol and its atmospheric dynamics at the Marseille–
695 Longchamp supersite, Atmos. Chem. Phys., 21, 7293–7319, https://doi.org/10.5194/acp-21-7293-2021, 2021.

Chazeau, B., El Haddad, I., Canonaco, F., Temime-Roussel, B., D'Anna, B., Gille, G., Mesbah, B., Prévôt, A. S. H., Wortham, H., and Marchand, N.: Organic aerosol source apportionment by using rolling positive matrix factorization: Application to a Mediterranean coastal city, Atmospheric Environment: X, 14, 100176, https://doi.org/10.1016/j.aeaoa.2022.100176, 2022a.

Chazeau, B., Haddad, I., Canonaco, F., Temime-Roussel, B., D'Anna, B., Gille, G., Mesbah, B., Prevot, A., Wortham, H., and
700 Marchand, N.: Organic aerosol source apportionment by using rolling positive matrix factorization: Application to a Mediterranean coastal city, Atmospheric Environment: X, 14, 100176, https://doi.org/10.1016/j.aeaoa.2022.100176, 2022b.

Chen, G., Sosedova, Y., Canonaco, F., Fröhlich, R., Tobler, A., Vlachou, A., Daellenbach, K. R., Bozzetti, C., Hueglin, C., Graf, P., Baltensperger, U., Slowik, J. G., El Haddad, I., and Prévôt, A. S. H.: Time-dependent source apportionment of submicron organic aerosol for a rural site in an alpine valley using a rolling positive matrix factorisation (PMF) window,
705 Atmos. Chem. Phys., 21, 15081–15101, https://doi.org/10.5194/acp-21-15081-2021, 2021.

Chen, G., Canonaco, F., Tobler, A., Aas, W., Alastuey, A., Allan, J., Atabakhsh, S., Aurela, M., Baltensperger, U., Bougiatioti, A., De Brito, J. F., Ceburnis, D., Chazeau, B., Chebaicheb, H., Daellenbach, K. R., Ehn, M., El Haddad, I., Eleftheriadis, K., Favez, O., Flentje, H., Font, A., Fossum, K., Freney, E., Gini, M., Green, D. C., Heikkinen, L., Herrmann, H., Kalogridis, A.-C., Keernik, H., Lhotka, R., Lin, C., Lunder, C., Maasikmets, M., Manousakas, M. I., Marchand, N., Marin, C., Marmureanu,
710 L., Mihalopoulos, N., Močnik, G., Nęcki, J., O'Dowd, C., Ovadnevaite, J., Peter, T., Petit, J.-E., Pikridas, M., Matthew Platt, S., Pokorná, P., Poulain, L., Priestman, M., Riffault, V., Rinaldi, M., Różański, K., Schwarz, J., Sciare, J., Simon, L., Skiba, A., Slowik, J. G., Sosedova, Y., Stavroulas, I., Styszko, K., Teinemaa, E., Timonen, H., Tremper, A., Vasilescu, J., Via, M., Vodička, P., Wiedensohler, A., Zografou, O., Cruz Minguillón, M., and Prévôt, A. S. H.: European aerosol phenomenology − 8: Harmonised source apportionment of organic aerosol using 22 Year-long ACSM/AMS datasets, Environment International,
715 166, 107325, https://doi.org/10.1016/j.envint.2022.107325, 2022.

Chirico, R., Prevot, A. S. H., DeCarlo, P. F., Heringa, M. F., Richter, R., Weingartner, E., and Baltensperger, U.: Aerosol and trace gas vehicle emission factors measured in a tunnel using an Aerosol Mass Spectrometer and other on-line instrumentation, Atmospheric Environment, 45, 2182–2192, https://doi.org/10.1016/j.atmosenv.2011.01.069, 2011.

Cohen, D. A. J.: Estimates and 25-year trends of the global burden of disease attributable to ambient air pollution: an analysis
720 of data from the Global Burden of Diseases Study 2015, 389, 12, 2017.

Crippa, M., Canonaco, F., Slowik, J. G., El Haddad, I., DeCarlo, P. F., Mohr, C., Heringa, M. F., Chirico, R., Marchand, N., Temime-Roussel, B., Abidi, E., Poulain, L., Wiedensohler, A., Baltensperger, U., and Prévôt, A. S. H.: Primary and secondary organic aerosol origin by combined gas-particle phase source apportionment, Atmospheric Chemistry and Physics, 13, 8411–8426, https://doi.org/10.5194/acp-13-8411-2013, 2013a.

725 Crippa, M., DeCarlo, P. F., Slowik, J. G., Mohr, C., Heringa, M. F., Chirico, R., Poulain, L., Freutel, F., Sciare, J., Cozic, J., Di Marco, C. F., Elsasser, M., Nicolas, J. B., Marchand, N., Abidi, E., Wiedensohler, A., Drewnick, F., Schneider, J., Borrmann, S., Nemitz, E., Zimmermann, R., Jaffrezo, J.-L., Prévôt, A. S. H., and Baltensperger, U.: Wintertime aerosol chemical composition and source apportionment of the organic fraction in the metropolitan area of Paris, Atmos. Chem. Phys., 13, 961–981, https://doi.org/10.5194/acp-13-961-2013, 2013b.

730 Cubison, M. J., Ortega, A. M., Hayes, P. L., Farmer, D. K., Day, D., Lechner, M. J., Brune, W. H., Apel, E., Diskin, G. S., Fisher, J. A., Fuelberg, H. E., Hecobian, A., Knapp, D. J., Mikoviny, T., Riemer, D., Sachse, G. W., Sessions, W., Weber, R. J., Weinheimer, A. J., Wisthaler, A., and Jimenez, J. L.: Effects of aging on organic aerosol from open biomass burning smoke

in aircraft and laboratory studies, Atmospheric Chemistry and Physics, 11, 12049–12064, https://doi.org/10.5194/acp-11-12049-2011, 2011.

735 Daellenbach, K. R., Uzu, G., Jiang, J., Cassagnes, L.-E., Leni, Z., Vlachou, A., Stefenelli, G., Canonaco, F., Weber, S., Segers, A., Kuenen, J. J. P., Schaap, M., Favez, O., Albinet, A., Aksoyoglu, S., Dommen, J., Baltensperger, U., Geiser, M., El Haddad, I., Jaffrezo, J.-L., and Prévôt, A. S. H.: Sources of particulate-matter air pollution and its oxidative potential in Europe, Nature, 587, 414–419, https://doi.org/10.1038/s41586-020-2902-8, 2020.

Dall'Osto, M., Paglione, M., Decesari, S., Facchini, M. C., O'Dowd, C., Plass-Duellmer, C., and Harrison, R. M.: On the
740 Origin of AMS "Cooking Organic Aerosol" at a Rural Site, Environ. Sci. Technol., 49, 13964–13972, https://doi.org/10.1021/acs.est.5b02922, 2015.

Dellinger, B., Pryor, W. A., Cueto, R., Squadrito, G. L., Hegde, V., and Deutsch, W. A.: Role of Free Radicals in the Toxicity of Airborne Fine Particulate Matter, Chem. Res. Toxicol., 14, 1371–1377, https://doi.org/10.1021/tx010050x, 2001.

Drewnick, F., Hings, S. S. S., Curtius, J., Eerdekens, G., and Williams, J.: Measurement of fine particulate and gas-phase species
745 during the New Year's fireworks 2005 in Mainz, Germany, Atmospheric Environment, 40, 4316–4327, https://doi.org/10.1016/j.atmosenv.2006.03.040, 2006.

Drinovec, L., Močnik, G., Zotter, P., Prévôt, A. S. H., Ruckstuhl, C., Coz, E., Rupakheti, M., Sciare, J., Müller, T., Wiedensohler, A., and Hansen, A. D. A.: The "dual-spot" Aethalometer: an improved measurement of aerosol black carbon with real-time loading compensation, Atmospheric Measurement Techniques, 8, 1965–1979, https://doi.org/10.5194/amt-8-
750 1965-2015, 2015.

Ducret-Stich, R. E., Tsai, M.-Y., Thimmaiah, D., Künzli, N., Hopke, P. K., and Phuleria, H. C.: PM10 source apportionment in a Swiss Alpine valley impacted by highway traffic, Environ Sci Pollut Res Int, 20, 6496–6508, https://doi.org/10.1007/s11356-013-1682-1, 2013.

Efron, B.: Bootstrap Methods: Another Look at the Jackknife, The Annals of Statistics, 7, 1–26,
755 https://doi.org/10.1214/aos/1176344552, 1979.

El Haddad, I., Marchand, N., Wortham, H., Piot, C., Besombes, J.-L., Cozic, J., Chauvel, C., Armengaud, A., Robin, D., and Jaffrezo, J.-L.: Primary sources of PM2.5 organic aerosol in an industrial Mediterranean city, Marseille, Atmos. Chem. Phys., 11, 2039–2058, https://doi.org/10.5194/acp-11-2039-2011, 2011.

El Haddad, I., D'Anna, B., Temime-Roussel, B., Nicolas, M., Boreave, A., Favez, O., Voisin, D., Sciare, J., George, C.,
760 Jaffrezo, J.-L., Wortham, H., and Marchand, N.: Towards a better understanding of the origins, chemical composition and aging of oxygenated organic aerosols: case study of a Mediterranean industrialized environment, Marseille, Atmos. Chem. Phys., 13, 7875–7894, https://doi.org/10.5194/acp-13-7875-2013, 2013.

Fang, Verma, V., Bates, J. T., Abrams, J., Klein, M., Strickland, M. J., Sarnat, S. E., Chang, H. H., Mulholland, J. A., Tolbert, P. E., Russell, A. G., and Weber, R. J.: Oxidative potential of ambient water-soluble PM2.5 in the southeastern United States:
765 contrasts in sources and health associations between ascorbic acid (AA) and dithiothreitol (DTT) assays, Atmos. Chem. Phys., 15, 2016.

Fang, T., Guo, H., Zeng, L., Verma, V., Nenes, A., and Weber, R. J.: Highly Acidic Ambient Particles, Soluble Metals, and Oxidative Potential: A Link between Sulfate and Aerosol Toxicity, Environ. Sci. Technol., 51, 2611–2620, https://doi.org/10.1021/acs.est.6b06151, 2017.

770 Flaounas, E., Coll, I., Armengaud, A., and Schmechtig, C.: The representation of dust transport and missing urban sources as major issues for the simulation of PM episodes in a Mediterranean area, Atmospheric Chemistry and Physics, 9, 8091–8101, https://doi.org/10.5194/acp-9-8091-2009, 2009.

Fröhlich, R., Cubison, M. J., Slowik, J. G., Bukowiecki, N., Prévôt, A. S. H., Baltensperger, U., Schneider, J., Kimmel, J. R., Gonin, M., Rohner, U., Worsnop, D. R., and Jayne, J. T.: The ToF-ACSM: a portable aerosol chemical speciation monitor
775 with TOFMS detection, Atmospheric Measurement Techniques, 6, 3225–3241, https://doi.org/10.5194/amt-6-3225-2013, 2013.

Gao, D., Godri Pollitt, K. J., Mulholland, J. A., Russell, A. G., and Weber, R. J.: Characterization and comparison of PM2.5 oxidative potential assessed by two acellular assays, Atmos. Chem. Phys., 20, 5197–5210, https://doi.org/10.5194/acp-20-5197-2020, 2020.

780 Grange, S. K., Uzu, G., Weber, S., Jaffrezo, J.-L., and Hueglin, C.: Linking Switzerland's PM10 and PM2.5 oxidative potential (OP) with emission sources, Aerosols/Field Measurements/Troposphere/Chemistry (chemical composition and reactions), https://doi.org/10.5194/acp-2021-979, 2022.

Grigas, T., Ovadnevaite, J., Ceburnis, D., Moran, E., McGovern, F. M., Jennings, S. G., and O'Dowd, C.: Sophisticated Clean Air Strategies Required to Mitigate Against Particulate Organic Pollution, Sci Rep, 7, 44737,
785 https://doi.org/10.1038/srep44737, 2017.

Grigoratos, T. and Martini, G.: Brake wear particle emissions: a review, Environ Sci Pollut Res, 22, 2491–2504, https://doi.org/10.1007/s11356-014-3696-8, 2015.

Henry, R., Norris, G. A., Vedantham, R., and Turner, J. R.: Source region identification using kernel smoothing, Environ Sci Technol, 43, 4090–4097, https://doi.org/10.1021/es8011723, 2009.

790 Hu, Y., Wu, M., Li, Y., and Liu, X.: Influence of PM1 exposure on total and cause-specific respiratory diseases: a systematic review and meta-analysis, Environ Sci Pollut Res Int, 29, 15117–15126, https://doi.org/10.1007/s11356-021-16536-0, 2022.

Jacob, D. J.: Chapter 11. Oxidizing Power of the Troposphere, Introduction to Atmospheric Chemistry, 199–219, 1999.

Kelly, F. J.: Education: Oxidative Stress: Its Role in Air Pollution and Adverse Health Effects, Occupational and Environmental Medicine, 60, 612–616, 2003.

795 Kiendler-Scharr, A., Mensah, A. A., Friese, E., Topping, D., Nemitz, E., Prevot, A. S. H., Äijälä, M., Allan, J., Canonaco, F., Canagaratna, M., Carbone, S., Crippa, M., Dall Osto, M., Day, D. A., De Carlo, P., Di Marco, C. F., Elbern, H., Eriksson, A., Freney, E., Hao, L., Herrmann, H., Hildebrandt, L., Hillamo, R., Jimenez, J. L., Laaksonen, A., McFiggans, G., Mohr, C., O'Dowd, C., Otjes, R., Ovadnevaite, J., Pandis, S. N., Poulain, L., Schlag, P., Sellegri, K., Swietlicki, E., Tiitta, P., Vermeulen, A., Wahner, A., Worsnop, D., and Wu, H.-C.: Ubiquity of organic nitrates from nighttime chemistry in the European submicron
800 aerosol, Geophysical Research Letters, 43, 7735–7744, https://doi.org/10.1002/2016GL069239, 2016.

Kumar, P., Robins, A., Vardoulakis, S., and Britter, R.: A review of the characteristics of nanoparticles in the urban atmosphere and the prospects for developing regulatory controls, Atmospheric Environment, 44, 5035–5052, https://doi.org/10.1016/j.atmosenv.2010.08.016, 2010.

Lelieveld, J., Evans, J. S., Fnais, M., Giannadaki, D., and Pozzer, A.: The contribution of outdoor air pollution sources to
805 premature mortality on a global scale, Nature, 525, 367–371, https://doi.org/10.1038/nature15371, 2015.

Lin, C., Ceburnis, D., Xu, W., Heffernan, E., Hellebust, S., Gallagher, J., Huang, R.-J., O'Dowd, C., and Ovadnevaite, J.: The impact of traffic on air quality in Ireland: insights from the simultaneous kerbside and suburban monitoring of submicron aerosols, Atmospheric Chemistry and Physics, 20, 10513–10529, https://doi.org/10.5194/acp-20-10513-2020, 2020.

810 Manigrasso, M., Costabile, F., Liberto, L. D., Gobbi, G. P., Gualtieri, M., Zanini, G., and Avino, P.: Size resolved aerosol respiratory doses in a Mediterranean urban area: From PM10 to ultrafine particles, Environment International, 141, 105714, https://doi.org/10.1016/j.envint.2020.105714, 2020.

Manousakas, M., Furger, M., Daellenbach, K. R., Canonaco, F., Chen, G., Tobler, A., Rai, P., Qi, L., Tremper, A. H., Green, D., Hueglin, C., Slowik, J. G., El Haddad, I., and Prevot, A. S. H.: Source identification of the elemental fraction of particulate matter using size segregated, highly time-resolved data and an optimized source apportionment approach, Atmospheric 815 Environment: X, 14, 100165, https://doi.org/10.1016/j.aeaoa.2022.100165, 2022a.

Manousakas, M., Furger, M., Daellenbach, K. R., Canonaco, F., Chen, G., Tobler, A., Rai, P., Qi, L., Tremper, A. H., Green, D., Hueglin, C., Slowik, J. G., El Haddad, I., and Prevot, A. S. H.: Source identification of the elemental fraction of particulate matter using size segregated, highly time-resolved data and an optimized source apportionment approach, Atmospheric Environment: X, 14, 100165, https://doi.org/10.1016/j.aeaoa.2022.100165, 2022b.

820 McGuire, M. L., Chang, R. Y.-W., Slowik, J. G., Jeong, C.-H., Healy, R. M., Lu, G., Mihele, C., Abbatt, J. P. D., Brook, J. R., and Evans, G. J.: Enhancing non-refractory aerosol apportionment from an urban industrial site through receptor modeling of complete high time-resolution aerosol mass spectra, Atmos. Chem. Phys., 14, 8017–8042, https://doi.org/10.5194/acp-14-8017-2014, 2014.

Medina S., Pascal M., and Tillier C.: Impacts de l'exposition chronique aux particules fines sur la mortalité en France 825 continentale et analyse des gains en santé de plusieurs scénarios de réduction de la pollution atmosphérique. Saint-Maurice, Santé Publique France, 2016.

Mohan, R.: Green bismuth, Nature Chem, 2, 336–336, https://doi.org/10.1038/nchem.609, 2010.

Møller, P.: Oxidative stress and inflammation generated DNA damage by exposure to air pollution particles, 34, 2014.

Münzel, T., Hahad, O., Sørensen, M., Lelieveld, J., Duerr, G. D., Nieuwenhuijsen, M., and Daiber, A.: Environmental risk 830 factors and cardiovascular diseases: a comprehensive expert review, Cardiovascular Research, 118, 2880–2902, https://doi.org/10.1093/cvr/cvab316, 2022.

Ng, N. L., Canagaratna, M. R., Jimenez, J. L., Zhang, Q., Ulbrich, I. M., and Worsnop, D. R.: Real-Time Methods for Estimating Organic Component Mass Concentrations from Aerosol Mass Spectrometer Data, Environ. Sci. Technol., 45, 910–916, https://doi.org/10.1021/es102951k, 2011.

835 Niranjan, R. and Thakur, A. K.: The Toxicological Mechanisms of Environmental Soot (Black Carbon) and Carbon Black: Focus on Oxidative Stress and Inflammatory Pathways, Front. Immunol., 8, 763, https://doi.org/10.3389/fimmu.2017.00763, 2017.

Nursanto, F. R., Meinen, R., Holzinger, R., Krol, M. C., Liu, X., Dusek, U., Henzing, B., and Fry, J. L.: What chemical species are responsible for new particle formation and growth in the Netherlands? A hybrid positive matrix factorization (PMF) 840 analysis using aerosol composition (ACSM) and size (SMPS), EGUsphere, 1–22, https://doi.org/10.5194/egusphere-2023-554, 2023.

Paatero, P.: The Multilinear Engine—A Table-Driven, Least Squares Program for Solving Multilinear Problems, Including the n-Way Parallel Factor Analysis Model, Journal of Computational and Graphical Statistics, 8, 854–888, https://doi.org/10.1080/10618600.1999.10474853, 1999.

845 Paatero, P. and Hopke, P. K.: Rotational tools for factor analytic models, Journal of Chemometrics, 23, 91–100, https://doi.org/10.1002/cem.1197, 2009.

Paatero, P. and Tapper, U.: Positive matrix factorization: A non-negative factor model with optimal utilization of error estimates of data values, Environmetrics, 5, 111–126, https://doi.org/10.1002/env.3170050203, 1994.

Pandolfi, M., Gonzalez-Castanedo, Y., Alastuey, A., de la Rosa, J. D., Mantilla, E., de la Campa, A. S., Querol, X., Pey, J., 850 Amato, F., and Moreno, T.: Source apportionment of PM10 and PM2.5 at multiple sites in the strait of Gibraltar by PMF: impact of shipping emissions, Environ Sci Pollut Res, 18, 260–269, https://doi.org/10.1007/s11356-010-0373-4, 2011.

Panko, J., Kreider, M., and Unice, K.: Chapter 7 - Review of Tire Wear Emissions: A Review of Tire Emission Measurement Studies: Identification of Gaps and Future Needs, in: Non-Exhaust Emissions, edited by: Amato, F., Academic Press, 147–160, https://doi.org/10.1016/B978-0-12-811770-5.00007-8, 2018.

855 Pant, P. and Harrison, R. M.: Estimation of the contribution of road traffic emissions to particulate matter concentrations from field measurements: A review, Atmospheric Environment, 77, 78–97, https://doi.org/10.1016/j.atmosenv.2013.04.028, 2013.

Pant, P., Baker, S. J., Shukla, A., Maikawa, C., Godri Pollitt, K. J., and Harrison, R. M.: The PM10 fraction of road dust in the UK and India: Characterization, source profiles and oxidative potential, Science of The Total Environment, 530–531, 445–452, https://doi.org/10.1016/j.scitotenv.2015.05.084, 2015.

860 Perrino, C., Tiwari, S., Catrambone, M., Torre, S. D., Rantica, E., and Canepari, S.: Chemical characterization of atmospheric PM in Delhi, India, during different periods of the year including Diwali festival, Atmospheric Pollution Research, 2, 418–427, https://doi.org/10.5094/APR.2011.048, 2011a.

Perrino, C., Tiwari, S., Catrambone, M., Torre, S. D., Rantica, E., and Canepari, S.: Chemical characterization of atmospheric PM in Delhi, India, during different periods of the year including Diwali festival, Atmospheric Pollution Research, 2, 418–865 427, https://doi.org/10.5094/APR.2011.048, 2011b.

Petit, J.-E., Favez, O., Sciare, J., Canonaco, F., Croteau, P., Močnik, G., Jayne, J., Worsnop, D., and Leoz-Garziandia, E.: Submicron aerosol source apportionment of wintertime pollution in Paris, France by double positive matrix factorization (PMF2) using an aerosol chemical speciation monitor (ACSM) and a multi-wavelength Aethalometer, Atmos. Chem. Phys., 14, 13773–13787, https://doi.org/10.5194/acp-14-13773-2014, 2014.

870 Petit, J.-E., Favez, O., Albinet, A., and Canonaco, F.: A user-friendly tool for comprehensive evaluation of the geographical origins of atmospheric pollution: Wind and trajectory analyses, Environmental Modelling & Software, 88, 183–187, https://doi.org/10.1016/j.envsoft.2016.11.022, 2017.

Piscitello, A., Bianco, C., Casasso, A., and Sethi, R.: Non-exhaust traffic emissions: Sources, characterization, and mitigation measures, Science of The Total Environment, 766, 144440, https://doi.org/10.1016/j.scitotenv.2020.144440, 2021.

875 Polissar, A. V., Hopke, P. K., Paatero, P., Malm, W. C., and Sisler, J. F.: Atmospheric aerosol over Alaska: 2. Elemental composition and sources, Journal of Geophysical Research: Atmospheres, 103, 19045–19057, https://doi.org/10.1029/98JD01212, 1998.

Polissar, A. V., Hopke, P. K., and Poirot, R. L.: Atmospheric aerosol over Vermont: chemical composition and sources, Environ Sci Technol, 35, 4604–4621, https://doi.org/10.1021/es0105865, 2001.

880 Pope, C. A.: Air Pollution and Health — Good News and Bad, N Engl J Med, 351, 1132–1134, https://doi.org/10.1056/NEJMe048182, 2004.

Rai, P., Furger, M., Slowik, J. G., Canonaco, F., Fröhlich, R., Hüglin, C., Minguillón, M. C., Petterson, K., Baltensperger, U., and Prévôt, A. S. H.: Source apportionment of highly time-resolved elements during a firework episode from a rural freeway site in Switzerland, Atmos. Chem. Phys., 20, 1657–1674, https://doi.org/10.5194/acp-20-1657-2020, 2020a.

885 Rai, P., Furger, M., Slowik, J. G., Canonaco, F., Fröhlich, R., Hüglin, C., Minguillón, M. C., Petterson, K., Baltensperger, U., and Prévôt, A. S. H.: Source apportionment of highly time-resolved elements during a firework episode from a rural freeway site in Switzerland, Atmos. Chem. Phys., 20, 1657–1674, https://doi.org/10.5194/acp-20-1657-2020, 2020b.

Rai, P., Furger, M., Slowik, J. G., Zhong, H., Tong, Y., Wang, L., Duan, J., Gu, Y., Qi, L., Huang, R. J., Cao, J., Baltensperger, U., and Prévôt, A. S. H.: Characteristics and sources of hourly elements in PM10 and PM2.5 during wintertime in Beijing,
890 Environmental Pollution, 116865 (11 pp.), https://doi.org/10.1016/j.envpol.2021.116865, 2021.

Reff, A., Eberly, S. I., and Bhave, P. V.: Receptor Modeling of Ambient Particulate Matter Data Using Positive Matrix Factorization: Review of Existing Methods, Journal of the Air & Waste Management Association, 57, 146–154, https://doi.org/10.1080/10473289.2007.10465319, 2007.

Roubicek, V., Raclavska, H., Juchelkova, D., and Filip, P.: Wear and environmental aspects of composite materials for
895 automotive braking industry, Wear, 265, 167–175, https://doi.org/10.1016/j.wear.2007.09.006, 2008.

Ryder, O. S., DeWinter, J. L., Brown, S. G., Hoffman, K., Frey, B., and Mirzakhalili, A.: Assessment of particulate toxic metals at an Environmental Justice community, Atmospheric Environment: X, 6, 100070, https://doi.org/10.1016/j.aeaoa.2020.100070, 2020.

Saffari, A., Hasheminassab, S., Wang, D., Shafer, M. M., Schauer, J. J., and Sioutas, C.: Impact of primary and secondary
900 organic sources on the oxidative potential of quasi-ultrafine particles (PM0.25) at three contrasting locations in the Los Angeles Basin, Atmospheric Environment, 120, 286–296, https://doi.org/10.1016/j.atmosenv.2015.09.022, 2015.

Salameh, D., Pey, J., Bozzetti, C., El Haddad, I., Detournay, A., Sylvestre, A., Canonaco, F., Armengaud, A., Piga, D., Robin, D., Prevot, A. S. H., Jaffrezo, J.-L., Wortham, H., and Marchand, N.: Sources of PM2.5 at an urban-industrial Mediterranean city, Marseille (France): Application of the ME-2 solver to inorganic and organic markers, Atmospheric Research, 214, 263–
905 274, https://doi.org/10.1016/j.atmosres.2018.08.005, 2018.

Shang, J., Jin, M., Chen, Y., Pan, Y., Li, Y., Tao, X., Cheng, Z., Meng, Q., Li, Q., Jia, G., Zhu, T., Hao, W., and Wei, X.: Comparison of lung damage in mice exposed to black carbon particles and 1,4-naphthoquinone coated black carbon particles, Science of The Total Environment, 580, https://doi.org/10.1016/j.scitotenv.2016.11.214, 2016.

Slowik, J. G., Vlasenko, A., McGuire, M., Evans, G. J., and Abbatt, J. P. D.: Simultaneous factor analysis of organic particle
910 and gas mass spectra: AMS and PTR-MS measurements at an urban site, Atmospheric Chemistry and Physics, 10, 1969–1988, https://doi.org/10.5194/acp-10-1969-2010, 2010.

Strak, M., Janssen, N. A. H., Godri, K. J., Gosens, I., Mudway, I. S., Cassee, F. R., Lebret, E., Kelly, F. J., Harrison, R. M., Brunekreef, B., Steenhof, M., and Hoek, G.: Respiratory Health Effects of Airborne Particulate Matter: The Role of Particle Size, Composition, and Oxidative Potential—The RAPTES Project, Environmental Health Perspectives, 120, 1183–1189,
915 https://doi.org/10.1289/ehp.1104389, 2012.

Sturm, R.: Modelling the deposition of fine particulate matter (PM 2.5) in the human respiratory tract, AME Medical Journal, 5, https://doi.org/10.21037/amj.2020.03.04, 2020.

Sun, Y., Wang, Z., Dong, H., Yang, T., Li, J., Pan, X., Chen, P., and Jayne, J. T.: Characterization of summer organic and inorganic aerosols in Beijing, China with an Aerosol Chemical Speciation Monitor, Atmospheric Environment, 51, 250–259,
920   https://doi.org/10.1016/j.atmosenv.2012.01.013, 2012.

Sylvestre, A., Mizzi, A., Mathiot, S., Masson, F., Jaffrezo, J. L., Dron, J., Mesbah, B., Wortham, H., and Marchand, N.: Comprehensive chemical characterization of industrial PM2.5 from steel industry activities, Atmospheric Environment, 152, 180–190, https://doi.org/10.1016/j.atmosenv.2016.12.032, 2017.

Tong, Y., Qi, L., Stefenelli, G., Wang, D. S., Canonaco, F., Baltensperger, U., Prévôt, A. S. H., and Slowik, J. G.:
925   Quantification of primary and secondary organic aerosol sources by combined factor analysis of extractive electrospray ionisation and aerosol mass spectrometer measurements (EESI-TOF and AMS), Atmospheric Measurement Techniques, 15, 7265–7291, https://doi.org/10.5194/amt-15-7265-2022, 2022.

Vecchi, R., Bernardoni, V., Cricchio, D., D'Alessandro, A., Fermo, P., Lucarelli, F., Nava, S., Piazzalunga, A., and Valli, G.: The   impact   of   fireworks   on   airborne   particles,   Atmospheric   Environment,   42,   1121–1132,
930   https://doi.org/10.1016/j.atmosenv.2007.10.047, 2008a.

Vecchi, R., Bernardoni, V., Cricchio, D., D'Alessandro, A., Fermo, P., Lucarelli, F., Nava, S., Piazzalunga, A., and Valli, G.: The   impact   of   fireworks   on   airborne   particles,   Atmospheric   Environment,   42,   1121–1132, https://doi.org/10.1016/j.atmosenv.2007.10.047, 2008b.

in 't Veld, M., Pandolfi, M., Amato, F., Pérez, N., Reche, C., Dominutti, P., Jaffrezo, J., Alastuey, A., Querol, X., and Uzu,
935   G.: Discovering oxidative potential (OP) drivers of atmospheric PM10, PM2.5, and PM1 simultaneously in North-Eastern Spain, Science of The Total Environment, 857, 159386, https://doi.org/10.1016/j.scitotenv.2022.159386, 2023.

Venables, W. N. and Ripley, B. D.: Modern applied statistics with S-Plus, 2nd ed., Springer, New York, 548 pp., 1997.

Verma, V., Fang, T., Guo, H., King, L., Bates, J. T., Peltier, R. E., Edgerton, E., Russell, A. G., and Weber, R. J.: Reactive oxygen species associated with water-soluble PM2.5 in the southeastern United States: spatiotemporal trends and source
940   apportionment, Atmos. Chem. Phys., 14, 12915–12930, https://doi.org/10.5194/acp-14-12915-2014, 2014.

Via, M., Yus-Díez, J., Canonaco, F., Petit, J.-E., Hopke, P. K., Reche, C., Pandolfi, M., Ivančič, M., Rigler, M., Prévôt, A. S. H., Querol, X., Alastuey, A., and Minguillón, M. C.: Towards a Better Understanding of Fine Pm Sources: Online and Offline Datasets Combination in a Single Pmf, https://doi.org/10.2139/ssrn.4370338, 2023.

Viana, M., Hammingh, P., Colette, A., Querol, X., Degraeuwe, B., Vlieger, I. de, and van Aardenne, J.: Impact of maritime
945   transport   emissions   on   coastal   air   quality   in   Europe,   Atmospheric   Environment,   90,   96–105, https://doi.org/10.1016/j.atmosenv.2014.03.046, 2014.

Visser, S., Slowik, J. G., Furger, M., Zotter, P., Bukowiecki, N., Canonaco, F., Flechsig, U., Appel, K., Green, D. C., Tremper, A. H., Young, D. E., Williams, P. I., Allan, J. D., Coe, H., Williams, L. R., Mohr, C., Xu, L., Ng, N. L., Nemitz, E., Barlow, J. F., Halios, C. H., Fleming, Z. L., Baltensperger, U., and Prévôt, A. S. H.: Advanced source apportionment of size-resolved
950   trace elements at multiple sites in London during winter, Atmospheric Chemistry and Physics, 15, 11291–11309, https://doi.org/10.5194/acp-15-11291-2015, 2015.

Waked, A., Favez, O., Alleman, L. Y., Piot, C., Petit, J.-E., Delaunay, T., Verlinden, E., Golly, B., Besombes, J.-L., Jaffrezo, J.-L., and Leoz-Garziandia, E.: Source apportionment of PM$_{10}$ in a north-western Europe regional urban background site (Lens,

France) using positive matrix factorization and including primary biogenic emissions, Atmospheric Chemistry and Physics,
955 14, 3325–3346, https://doi.org/10.5194/acp-14-3325-2014, 2014.

Weber, S., Uzu, G., Calas, A., Chevrier, F., Besombes, J.-L., Charron, A., Salameh, D., Ježek, I., Močnik, G., and Jaffrezo, J.-L.: An apportionment method for the oxidative potential of atmospheric particulate matter sources: application to a one-year study in Chamonix, France, Atmos. Chem. Phys., 18, 9617–9629, https://doi.org/10.5194/acp-18-9617-2018, 2018.

Weber, S., Salameh, D., Albinet, A., Alleman, L. Y., Waked, A., Besombes, J.-L., Jacob, V., Guillaud, G., Meshbah, B., Rocq,
960 B., Hulin, A., Dominik-Sègue, M., Chrétien, E., Jaffrezo, J.-L., and Favez, O.: Comparison of PM10 Sources Profiles at 15 French Sites Using a Harmonized Constrained Positive Matrix Factorization Approach, Atmosphere, 10, 310, https://doi.org/10.3390/atmos10060310, 2019a.

Weber, S., Salameh, D., Albinet, A., Alleman, L. Y., Waked, A., Besombes, J.-L., Jacob, V., Guillaud, G., Meshbah, B., Rocq, B., Hulin, A., Dominik-Sègue, M., Chrétien, E., Jaffrezo, J.-L., and Favez, O.: Comparison of PM10 Sources Profiles at 15
965 French Sites Using a Harmonized Constrained Positive Matrix Factorization Approach, Atmosphere, 10, 310, https://doi.org/10.3390/atmos10060310, 2019b.

Weber, S., Uzu, G., Favez, O., Borlaza, L. J. S., Calas, A., Salameh, D., Chevrier, F., Allard, J., Besombes, J.-L., Albinet, A., Pontet, S., Mesbah, B., Gille, G., Zhang, S., Pallares, C., Leoz-Garziandia, E., and Jaffrezo, J.-L.: Source apportionment of atmospheric PM10; oxidative potential: synthesis of 15 year-round urban datasets in France, Atmos. Chem. Phys., 21, 11353–
970 11378, https://doi.org/10.5194/acp-21-11353-2021, 2021.

World Health Organization : 7 million premature deaths annually linked to air pollution: https://www.who.int/mediacentre/news/releases/2014/air-pollution/en/, last access: 12 April 2021.

World Health Organization : Particules atmosphériques, Cycle des particules atmosphériques - Encyclopædia Universalis: https://www.universalis.fr/encyclopedie/particules-atmospheriques/3-cycle-des-particules-atmospheriques/, last access: 12
975 April 2023.

Xu, L., Suresh, S., Guo, H., Weber, R. J., and Ng, N. L.: Aerosol characterization over the southeastern United States using high-resolution aerosol mass spectrometry: spatial and seasonal variation of aerosol composition and sources with a focus on organic nitrates, Atmospheric Chemistry and Physics, 15, 7307–7336, https://doi.org/10.5194/acp-15-7307-2015, 2015.

Yu, H., Wei, J., Cheng, Y., Subedi, K., and Verma, V.: Synergistic and Antagonistic Interactions among the Particulate Matter
980 Components in Generating Reactive Oxygen Species Based on the Dithiothreitol Assay, Environ. Sci. Technol., 52, 2261–2270, https://doi.org/10.1021/acs.est.7b04261, 2018.

Yu, S., Liu, W., Xu, Y., Yi, K., Zhou, M., Tao, S., and Liu, W.: Characteristics and oxidative potential of atmospheric PM2.5 in Beijing: Source apportionment and seasonal variation, Science of The Total Environment, 650, 277–287, https://doi.org/10.1016/j.scitotenv.2018.09.021, 2019.

985 Zhang, X., Staimer, N., Tjoa, T., Gillen, D. L., Schauer, J. J., Shafer, M. M., Hasheminassab, S., Pakbin, P., Longhurst, J., Sioutas, C., and Delfino, R. J.: Associations between microvascular function and short-term exposure to traffic-related air pollution and particulate matter oxidative potential, Environ Health, 15, 81, https://doi.org/10.1186/s12940-016-0157-5, 2016.

Zhuang, H., Chan, C. K., Fang, M., and Wexler, A. S.: Formation of nitrate and non-sea-salt sulfate on coarse particles, Atmospheric Environment, 33, 4223–4233, https://doi.org/10.1016/S1352-2310(99)00186-7, 1999.

990   Zografou, O., Gini, M., Manousakas, M. I., Chen, G., Kalogridis, A. C., Diapouli, E., Pappa, A., and Eleftheriadis, K.:
Combined organic and inorganic source apportionment on yearlong ToF-ACSM dataset at a suburban station in Athens,
Atmospheric Measurement Techniques, 15, 4675–4692, https://doi.org/10.5194/amt-15-4675-2022, 2022.